TRI-AXIAL ELECTROSPINNING WITH BLOCK COPOLYMERS AND SILICA PRECURSOR

A Thesis

Presented to the Faculty of the Graduate School

of Cornell University

in Partial Fulfillment of the Requirements for the Degree of

Master of Science

by

Jay Hoon Park

August 2009

ABSTRACT

Multi-layered nanofibers have been produced via electrospinning with block copolymer (polystyrene-*b*-polyisoprene, PS-*b*-PI) solution sandwiched between innermost and outermost silica precursor layers. The purpose of tri-axial approach is to investigate the effect of the interfacial interaction and physical confinement on the self-assembly in electrospun nanofibers.

A novel tri-axial electrospinning setup based on a serial connection of two needles with side feeding has been devised first, and PS-*b*-PI systems of both asymmetric and symmetric morphology with and without surface-modified, magnetite nanoparticles have been studied. The results reveal that confined-assembly is changed significantly by the presence and interaction with both inner and outer silica layers. The incorporation of nanoparticles also revealed that PI phase is wetted against the silica wall, on the contrary to previous reports on PS-*b*-PI/silica coaxial nanofibers where PS phase is wetted against the silica sheath. The same migration of PI phase to the silica layers has been observed when a blend of pure PS and PS-*b*-PI was used as a middle layer.

To investigate the mechanics behind confinement and wall interaction, coarse-grained molecular dynamics (MD) simulation of model symmetric block copolymer (BCP) in cylindrical confinement has been assessed. The simulation results under cylindrical confinement without preference of polymer domains to the wall exhibit stacked lamellae along the fiber axis which was also observed in coaxial electrospun nanofibers of symmetric PS-*b*-PI. It is also predicted that nanoparticles with selective

interaction towards one of BCP domains tend to migrate towards the wall when they are incorporated into BCP under confinement.

Multi-layered nanofibers developed in the current study can provide further insights on the effect of confinement and wall interactions on various self-assembly systems including block copolymer-inorganic hybrid materials. The devised tri-axial approach can also be employed to fabricate multi-layered, multi-structured nanofibers for high end applications such as drug delivery.

BIOGRAPHICAL SKETCH

Jay Hoon Park was born in Urbana, IL on January 8th, 1983. A month later, he moved to Seoul, Korea and lived there until August 1995. He then moved to Blacksburg, VA to attend Blacksburg Middle School and Blacksburg High School from August 1995 to May 2000. He attended Johns Hopkins University in Baltimore, MD from August 2000 to May 2004. He was conferred the degree of Bachelor or Sciences in Chemical Engineering in May 2004, and he went back to Seoul, Korea until August 2006. There, he has worked as a research assistant in Seoul National University under Dr. Seung Woo Park from January to August 2006 while preparing for graduate school. He started to attend Cornell University for Masters of Engineering in Chemical and Bimolecular Engineering from August 2006 to May 2007. Then, he started to pursue Masters of Science program in Chemical and Biomolecular Engineering.

to my wife and parents

ACKNOWLEDGMENTS

I'd like to thank my advisor, Dr. Yong L. Joo, for his immense help in getting me started with this project, and giving me numerous invaluable advices throughout the courses of the research. I also like to thank Dr. Margaret Frey for her role in Special Committee and her advices on the project.

I would like to thank Dr. Jeanne Panels for helping with designs of tri-axial electrospinning setup. I also want to thank Dr. Vibha Kalra for advices from her coaxial electrospinning experiences and molecular dynamics simulations. And I want to thank Dr. Jung Hun Lee for his contributions in experiments and nanoparticle production. I also would like to thank the other members of Joo group, Nate Hansen and Dr. Dae Hwan Cho. I also want to express my gratitude to John Grazul for assistances in using Tecnai T-12, and Dr. Yuanming Zhang for assistances in using Leica Ultramicrotome.

Finally, I want to thank my family and friends for their support and guidance.

TABLE OF CONTENTS

LIST OF FIGURES

LIST OF TABLES

CHAPTER 1

INTRODUCTION

1.1. Block Copolymers (BCP)

Block copolymers are macromolecules composed of sequences, or blocks, of chemically distinct repeat units [1]. The block copolymers are typically developed using termination-free anionic polymerization, which is the sequential addition of monomers of various carbanion-terminated linear polymer chains. When two distinct monomer types(e.g. isoprene and styrene) are polymerized, it is referred to as *AB* block copolymers. This class of block copolymers has a variety of possible molecular architectures. One example is obtained by the two-step anionic polymerization of *A* and *B* monomers, also known as *A-B* diblock copolymer. There are more complicated structures that involve a three-step reaction such as *ABA* or *BAB* triblock copolymer. It is also possible to have a "living" diblock copolymer react with other diblock or triblock copolymer to produce $(A\text{-}B)_n$ star-block copolymers. The representative $(A\text{-}B)_n$ architectures are illustrated in Figure 1.1. As a consequence of the "living" nature of these reactions, the resulting block and overall molecular weight distributions are nearly ideal, i.e. $M_w / M_n < 1.1$, where M_w and M_n represent the weight and number-average molecular weights, respectively [1]. A variety of new polymerization methods have evolved since the anionic block copolymerization which originated in 1950s [2,3]. Methods such as Ziegler Natta and condensation polymerization have contributed to an expanding number of block copolymer classes (e.g. *ABC*) and novel architectures (e.g. graft-block) [1, 4, 5]. However, anionic polymerization remains the only viable method for producing mono disperse block copolymers with well-defined structures [1]. And thus most current theories deal with model $(A\text{-}B)_n$ type block copolymers.

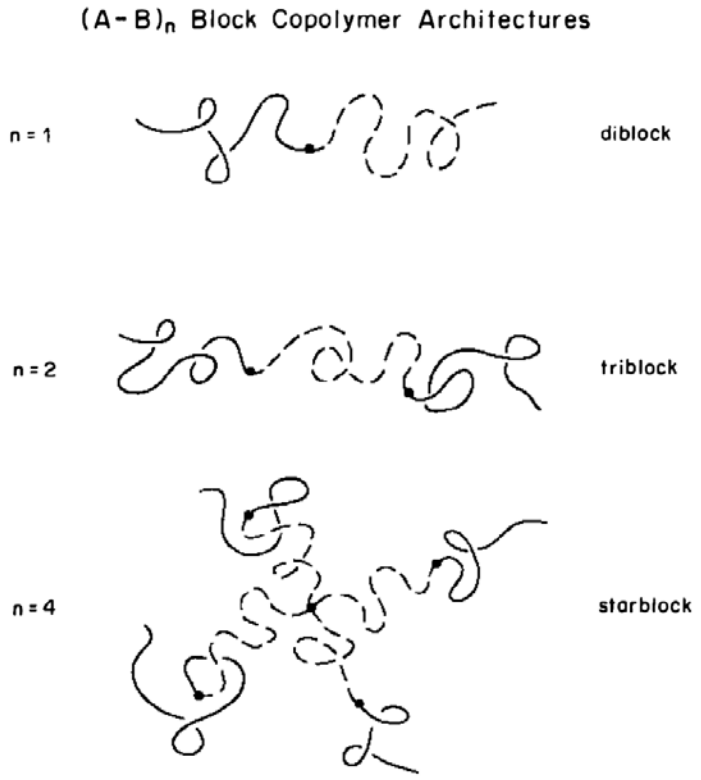

Figure 1.1: Schematic illustration of several $(A\text{-}B)_n$ type block copolymer architectures. Solid and dashed lines represent A and B block chains. The $n = 1$ and $n = 2$ architectures are commonly referred to as diblock and triblock copolymers, while $n \geq 3$ are denoted starblock copolymers [1].

1.2. Self-assembly

In general, the phase behavior of bulk $(A\text{-}B)_n$ block copolymers is determined by three experimentally controllable factors: the overall degree of polymerization N, architectural constraints characterized by n and the composition f (overall volume fraction of the A component), and the $A\text{-}B$ segment-segment (Flory-Huggins) interaction parameter χ [1]. The composition f and N are regulated through the polymerization stoichiometry and influence the translational and configurational entropy, whereas the magnitude of χ is determined by the selection of the $A\text{-}B$ monomer pair. For most system, the interaction parameter has the temperature

dependence $\chi \approx \alpha T^{-1} + \beta$, where $\alpha > 0$ and β are constants for given values of f and n. At equilibrium, a dense collection of monodisperse diblock copolymer chains will be arranged in minimum free energy configurations. Increasing the energy parameter χ (hence reducing the temperature) favors a reduction in A-B monomer contacts. If N is sufficiently large, this may be accomplished with some loss of translational and configurational entropy by local compositional ordering [1]. Such local segregation is often referred to as microphase separation, for a macroscopic phase separation is impossible in a single-component block copolymer due to the different components being tethered together [1]. If either χ or N is decreased enough, the entropic factors will dominate, leading to a compositionally disordered phase. The entropic contribution to the free energy density scales as N^1, while that of the enthalpic contribution scales as χ. Thus, it is the product χN that dictates the block copolymer phase state [1]. The relationship between the product χN and f results in the self-assembly of BCPs into various morphologies such as lamellae, spheres, rods, cylinders, and bicontinous phases. Figure 1.2 illustrates the relationship between χN and volume fraction and its resulting morphologies.

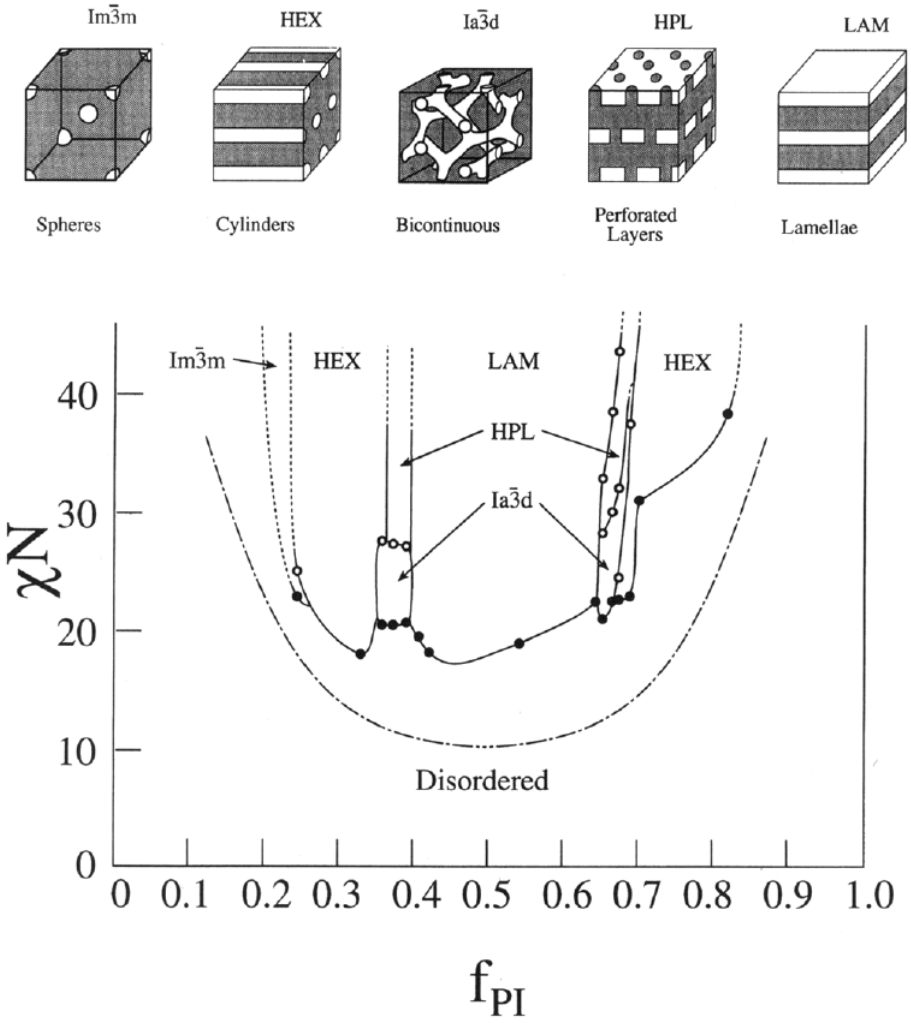

Figure 1.2: Phase diagram for PI-PS diblock copolymers (χN versus f_{PI}). Open and filled circles represent the order-order (OOT) and order-disorder (ODT) transitions, respectively. The dash-dot curve is the mean field prediction for the ODT. Solid curves have been drawn to delineate the different phases observed but might not correspond to precise phase boundaries. Five different ordered microstructures (shown schematically) have been observed for this chemical system [6].

1.3. Confined Assembly

Several researches have been done in attempt to study self-assembly of BCP under the effect of confinement of self-assembling materials in 1D nanostructure (such as nanorods, nanowires, etc.) [7,8,9]. Shin *et al.* [8] and Xiang *et al.* [9] studied the effect of cylindrical confinement on the morphology of polystyrene-*block*-polybutadiene

(PS-*b*-PBD) in nanoporous alumina membranes (Figure 1.3).

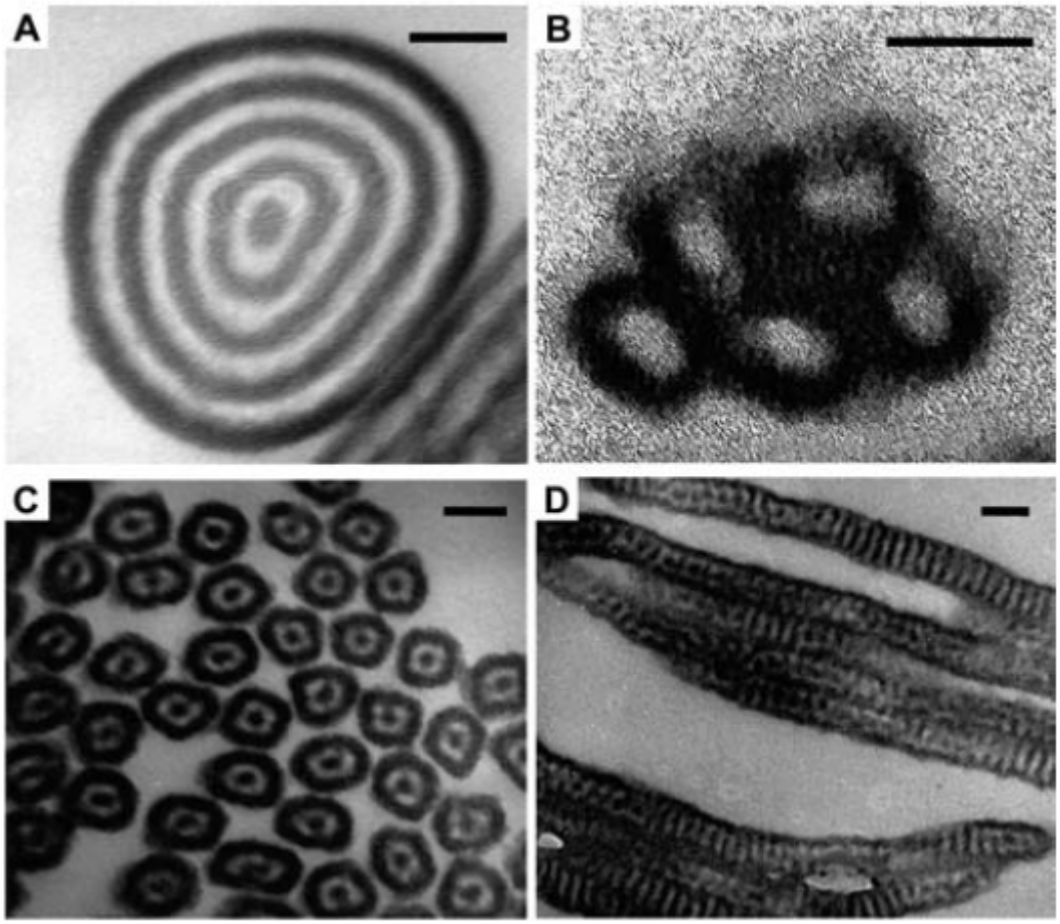

Figure 1.3: (A to D) TEM images of PS-b-PBD nanorods from a nanoporous alumina membrane. The pore diameters d and lamellar repeating periods L0 are (A) 190 and 23.5 nm, (B) 45 and 23.5 nm, and both (C) and (D), 45 and 17.6 nm, respectively. (A), (B), and (C) are cross-sections cut normal to the rod axis, and (D) is a cross section parallel to the rod axis. Scale bars, 50 nm [8].

They cylindrically confined the block copolymer in nanoporous alumina membrane, and dissolved the membrane with weak base after annealing [7,8]. They found that if the pore diameter is large compared to the equilibrium bulk spacing and one component preferentially segregates to the walls, then a symmetric copolymer forms with a concentric cylindrical morphology and alternating cylinders of PS and PBD. High degree of curvature imposed in the cylindrical confinement eventually leads to

frustration of chain packing at the interface, forming stacked PS lamellar morphology along the pore axis. Wu *et al.* [10] studied the confined assembly of SiO_2/copolymer-composite mesostructures in cylinders of varying diameters using alumina nanochannels. They also carried out self-consistent field calculations for comparison with experimentally obtained self-assembled structures.

1.4. Interaction of Nanoparticle(NP) with BCP

Controlling the spatial location of NP in polymer matrices is the fundamental challenge surrounding the development of high-end polymer nanocomposite materials. High particle surface energies and strong interparticle interactions often lead to particle aggregation, making it difficult to control their location. Typically, the nanoparticle surfaces are modified to avoid aggregates and ensure homogenous distribution throughout the polymer material. However, the effectiveness of these NPs can be enhanced if they are arranged periodically in three dimensions. One can combine the functionality of NPs with the phenomena of BCP self-assembly to achieve hierarchical spatial distributions of NPs [11]. Having the NPs periodically spaced can lead to synergistic effects of optical and mechanical properties, for example, and can potentially be used in novel applications such as magnetic storage media and catalysis [12,13].

Recently, there have been numerous studies on self-assembly of block copolymer and NP in quiescent systems. These works were performed as a function of various parameters, such as NP surface modification, size of NPs relative to polymer radius of gyration, and volume fraction of NPs in the composite. Some of these studies focused on enthalpic interactions of polymer matrices and NP. For example, Chui *et al.* [14] placed selective gold nanoparticles in the polystyrene domain of symmetric

Poly(styrene-b-2 vinyl pyridine) (PS-PVP) diblock copolymer by coating them with PS ligands. In contrast, particles coated with mixtures of PS and PVP localized at the interfaces between the PS-PVP blocks. Shultz *et al.* reported qualitatively similar results by using discontinuous molecular dynamics simulations [15]. There are also some studies done on the effect of entropic factors on the displacement of NPs. There are two main competing entropic forces affecting the displacement of NPs, namely the entropic penalty of chain stretching and the translational entropy of NPs. The chain stretching entropic penalty plays big role for large selective particles if the particles are uniformly dispersed in the preferred domain, resulting in NPs being pushed towards the chain ends at the center of the domain even with the loss in the translational entropy of the NPs. For nanoparticles that are small compared to the polymer radius of gyration, particle translational entropy dominates and they are uniformly dispersed in the preferred domain [13,16].

Surface modified NPs in BCPs can cause a significant increase in its domain size, eventually resulting in change of morphology. Sides *et al.* [17] showed both experimentally and using hybrid particle field simulations that on increasing the NP volume fraction in a lamellar-forming diblock copolymer, the preferred domain becomes swollen and distorted and finally transforms into inverse hexagonal cylinder morphology to minimize interfacial energy. Although surface modification has played an important role in guiding the NPs to desired locations in block copolymers for many metals such as gold and silver, in the case of magnetically active particles like magnetite, strong magnetic dipole interactions between particles often lead to clustering and aggregation [18,19]. Magnetite can display high saturation magnetization and resistance to oxidation, attracting great interest for electrical and biomedical applications. Magnetite nanoparticles have also been shown to display

superparamagnetic behavior due to their small size, making them ideal for magnetic field driven transport of drugs, bioseparations, electromagnetic shielding, and magnetic sensing [18,19,20]. Park *et al.* [21] exploited the selectivity of film casting solvents to control the morphology of magnetic NP/polystyrene-block-polyisoprene (PS-b-PI) nanocomposite films. They used monodisperse g-Fe2O3 nanoparticles of 7-nm diameter with surfaces modified with oleic acid making them marginally selective towards PI. For solvents such as tetrahydrofuran (THF) and toluene, which are neutral towards PS and PI, they reported the formation of lattice-like NP aggregates beyond a small weight fraction of 0.02. For PI selective solvents like hexane, they were able to selectively incorporate NPs into the PI phase; however, aggregates were formed and selectivity of NPs was lost above a weight fraction of 0.05.

1.5. Electrospinning

Electrospinning is a novel process which creates submicron to micron scaled fibers from polymer solutions using electrical forces. When electricity is applied to the tip of the spinneret to create an electrical field gradient between a polymer solution and the grounded collector, the solution forms a pendant-like droplet known as Taylor cone [22]. It is supported by surface tension at the tip of the spinneret, and when the electrical gradient between the tip of the solution and the collector overcomes the surface tension, a fine, charged jet is ejected. This jet is elongated greatly as the electric force is increased which is said to contribute to the small diameters of electrospun fibers. The ejected jet then undergoes deformation (strain (extension) rate ~10000 s^{-1}) and rapidly evaporates (~ 200 nl/s), resulting in solidified fiber accumulated on the grounded collector [23]. Typical process of electrospinning is depicted in Figure 1.4.

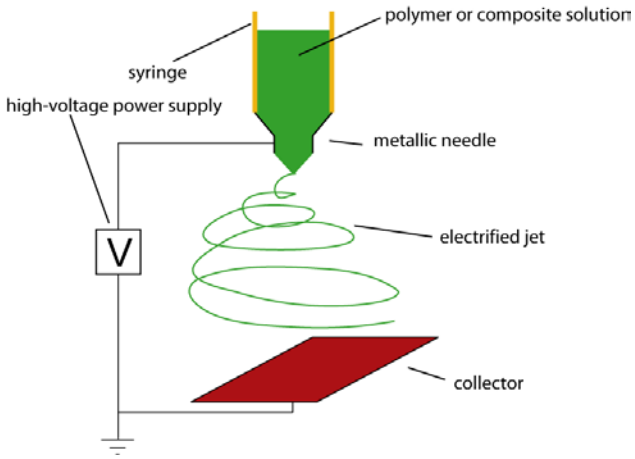

Figure 1.4: Typical schematic of electrospinning

These electrospun fibers are widely used as high performance separation, sensing, and filtration devices because of their large surface area to mass ratio, where typical specific surface area is 10 m^2/g for fiber diameters around 500 nm and 1000 m^2/g for diameters around 50 nm [24]. Electrospun nanofibers also have their applications in biomedical areas as artificial organ components, implant materials, medical textile materials, wound dressing, and vehicles in drug delivery. These fibers also have a potential to be used as a substrate for enzyme immobilization [25].

There are several process variables in electrospinning. These variables include i) molecular weight and architecture of the polymer, ii) solution properties such as viscosity, conductivity and surface tension, iii) processing conditions including electric potential, flow rate, distance between the capillary and the collection screen, and iv) ambient parameters such as temperature, humidity and air velocity. These variables have a direct impact on the product, such as the diameter and morphology of fibers. Viscosity is one of the most critical variables among the aforementioned factors. Electrospinnable solution typically requires to be in a viscosity range of 10 ~1000

Poise. If the solution viscosity is too low, the solution will undergo electrospraying to form discontinuous jets during the process, or form beads. If the viscosity of solution is too high, the formation of fibers will not be viable as the tip of the solution will clog up and unable to form thin jet [26].

Recently, there have been some electrospinning studies utilizing block copolymers. Fong *et al.* [27] produced nanofibers from styrene-butadienestyrene triblock copolymer solution by electrospinning. They observed weak and irregular microphase separation on the surface of electrospun fibers. They found that annealing of fibers allowed the phase domains to become larger. Ma *et al.* [28] produced super hydrophobic microphase-separated nanofibers from solution of poly(styrene-*block*-dimethylsiloxane) block copolymer blended with homopolymer PS in THF and dimethylformamide via electrospinning. They reported the formation of PDMS cylinders in PS matrix via TEM. Self-assembly of comb-shaped supermolecules, polystyrene-*block*-poly(4- inylpyridine) (PS-*b*-P4VP(PDP)-pentadecylphenol(PDP), in electrospun fibers has also been studied [29].

Self-assembly of the BCPs has thoroughly been studied for bulk film systems by theory, experiments, and simulations. Control over the morphologies in size and shape is desired to be widely used in nanoscale system applications. While the self-assembly study of BCPs in bulk created numerous potential applications for distinctive nanostructures, they are limited by their short length scale and difficulty in separating the nanostructures from the supporting BCP films. In this effort to obtain novel morphologies in confined yet continuous and long nanostructures, Kalra *et al.* recently reported the structure development in polystyrene-*block*-polyisoprene (PS-*b*-PI) nanofibers formed via electrospinning [30]. When the BCP/THF solutions were electrospun, microphase separations with incomplete and disconnected domain

structures were observed in as-electrospun PS-*b*-PI nanofibers due to extreme deformation[31,32,33] and rapid evaporation[34] that occur during electrospinning. These as-spun fibers could return to its self-assembling morphology by means of thermal annealing. However, such a process usually requires the annealing temperature to be higher than glass transition temperature of the polymer, leading to disruption of the fiber morphology. Figure 1.5 shows results from the electrospinning and annealing of electrospun PS-*b*-PI nanofibers.

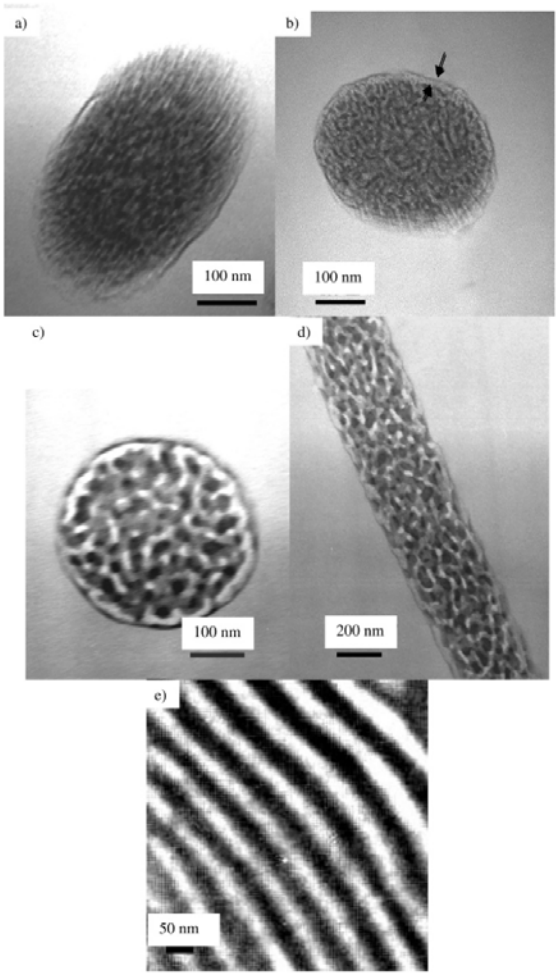

Figure 1.5: TEM images of IS53 copolymer: (a, b) two cross sections with different domain structures of fiber spun from 25 wt % solution in THF; (c) cross section of fiber annealed at 90 °C for 12 h; (d) along the axis of fiber annealed at 90 °C for 12 h; (e) film cast from 10 wt % solution in THF [30]

In order to accommodate for such difficulties, thermally stable materials such as silica is used as a sheath to preserve the fiber morphology during the post annealing treatment [35]. To do this, one has to prepare such silica precursor solution for a sol-gel process, and coaxially electrospin the polymer solution and the silica precursor, as core and skin layer, respectively. The sol-gel process and the coaxial electrospinning are discussed further in detail in the following sections.

1.6. Sol-gel Synthesis

A sol is a colloidal suspension of nanometer-sized solid particles in a liquid, such as blood and pigmented ink. Over time, the sols crosslink with each other to form an integrated network called a gel. The transition process of the sol evolving into gel is called sol-gel, where in the present study the sol is the silica precursor that eventually becomes a gel of silica [34]. The silica is usually electrospun at this sol-gel phase, when its viscosity reaches 10 Poise.

The silica sol-gel is typically made from a silica precursor oxide, such as tetra(ethyl)ortho-silicate(TEOS), with combination of ethanol. The TEOS/ethanol solution is then added by a water and small amount of acidic catalyst such as HCl to undergo hydrolysis and condensation reactions. An acid catalyst is used in fiber spinning processes because it produces linear structures, while a basic catalyst tends to form colloidal particles. The more linear the material, the easier it is to spin [37]. The reaction scheme is shown in Figure 1.6, and as the TEOS/ethanol sol evolves towards gel, the viscosity increases, eventually reaching the desirable viscosity to be used in electrospinning.

a) $(RO)_4Si + nH_2O \longrightarrow (RO)_4\text{-}nSi(OH)_n + ROH$

b) $Si(OH)_4 + nROH \longleftrightarrow Si(OH)_{4-n}(OR)_n + nH_2O$

Figure 1.6: Reaction scheme of sol-gel synthesis a) hydrolysis reaction and b) condensation reaction [38]

The composition of the sol also affects how well the solution can be electrospun. Figure 1.7 shows composition of silica sol-gel and its affect on the spinnability of the solution in conventional fiber spinning. This is because water and ethanol largely influence the hydrolysis and condensation reaction. For the best conditions for electrospinning, molar ratios of water to TEOS between 1 and 4 are selected. When the solution reaches viscosity about10 Poise, it is ready to be electrospun, while keeping in mind that viscosity eventually increases as sol evolves further towards gel, rendering the solution too viscous to spin.

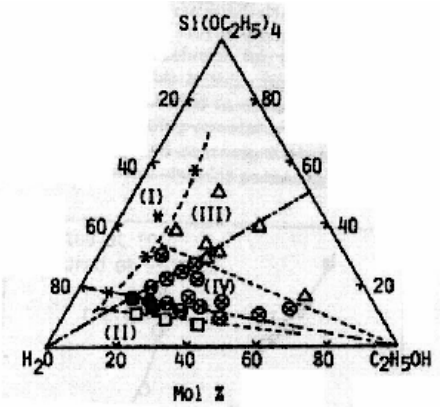

Figure 1.7: Relationship between fiber drawing behavior and composition of silica fibers. Area I: immiscible, Area II: not spinnable, Area III: no gel formation, Area IV: spinnable region [26]

been achieved using conventional spinning methods [26]. Silica nanofiber mats can be produced through a sol-gel synthesis/electrospinning technique without using any polymer binder [39]. In addition, silica nanofiber mats also provide an ideal platform

for the incorporation of transition metal particles [40]. Various metal alkoxides can be included by adding them to the sol-gel precursor [36]. When the viscosity of the solution reaches a certain range (10 to 1000 Poise) it may be electrospun [26]. Panels presented an electrospun silica mats containing vanadium pentoxide for its gas sensing capabilities [36]. Prior to this work, thin films containing V_2O_5 were used for sensing toxic or flammable gases such as ammonia, but this method only utilizes the surface layer of the film because the gas flows over the film [41, 42]. Nanofiber mats provide a highly porous template where the gas can flow through it, and thereby effectively utilize the entire active sites on the fibers [36].

In present study, the silica sol-gel is prepared by condensation and hydrolysis reactions in a selected molar ratio of TEOS:EtOH:H2O:HCl of 1:2:2:0.01 was used. The solution is cooked under a moderate temperature of 50°C for 3~5 hours when it reaches a spinnable viscosity of about 10 poise. The viscosity along with the high electric conductivity of the solvent helps the formation of very stable liquid jets in the presence of electric field and robust nanofibers [36].

1.7. Coaxial Electrospinning

The coaxial electrospinning typically consists of two different immiscible liquids placed in a coaxial spinneret, which ultimately creates core/sheath nanofibers. Sun *et al.* [43] utilized combination of polymer solution and melt, demonstrating the undesirable mixing of two layers is prevented by the rapid evaporation when compared to the slower diffusion rate between the polymers. As Yu *et al.* [44] have demonstrated, the shell layer serves as a template for formation of fibers along with the core material. In other words, a relatively less viscoelastic material that is usually hard to electrospin by itself can be spun into fiber by help of more viscoelastic shell

layer. Thus, in the present study the silica shell also serves as a process aid for low molecular weight unentangled polymers that are normally difficult or impossible to electrospin in addition to providing a thermally stable sheath to the core BCP solution. Typical coaxial electrospinning setup is demonstrated in Figure 1.8.

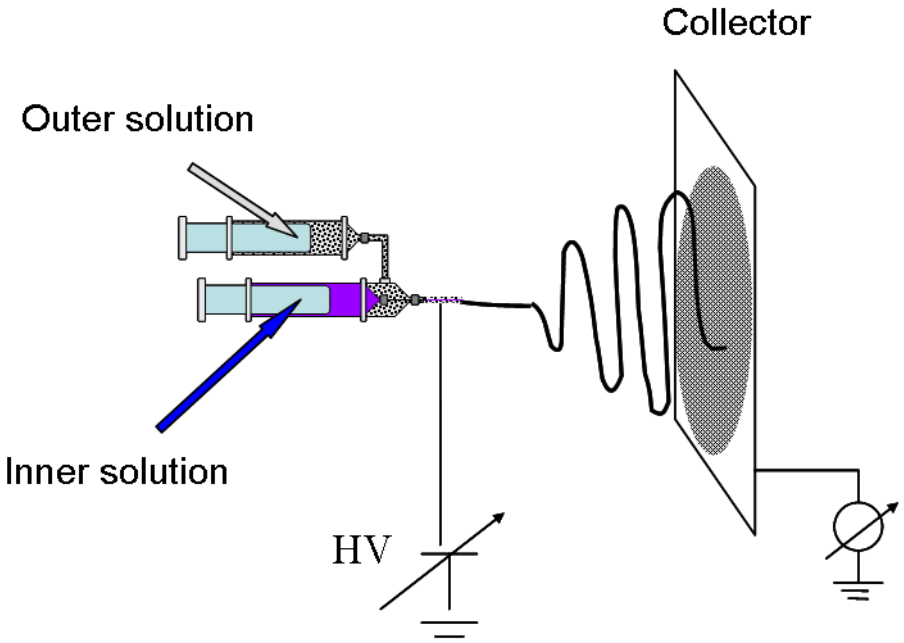

Figure 1.8: Typical coaxial electrospinning setup [35]

Kalra *et al.* demonstrated the cylindrical confinement effect of BCPs using BCP solution in core and silica as outer layer [35]. With the silica layer present, high temperature annealing treatment could be done to the as-spun fibers. The post annealing treatment of such coaxial nanofibers recovered the original morphologies of BCP [8]. Figure 1.9 demonstrates PS-*b*-PI BCP nanofibers that originally self assemble into lamellae in bulk film have morphology with non-uniform microphase separation in as-spun fibers, but recover their concentric lamella rings form after annealing.

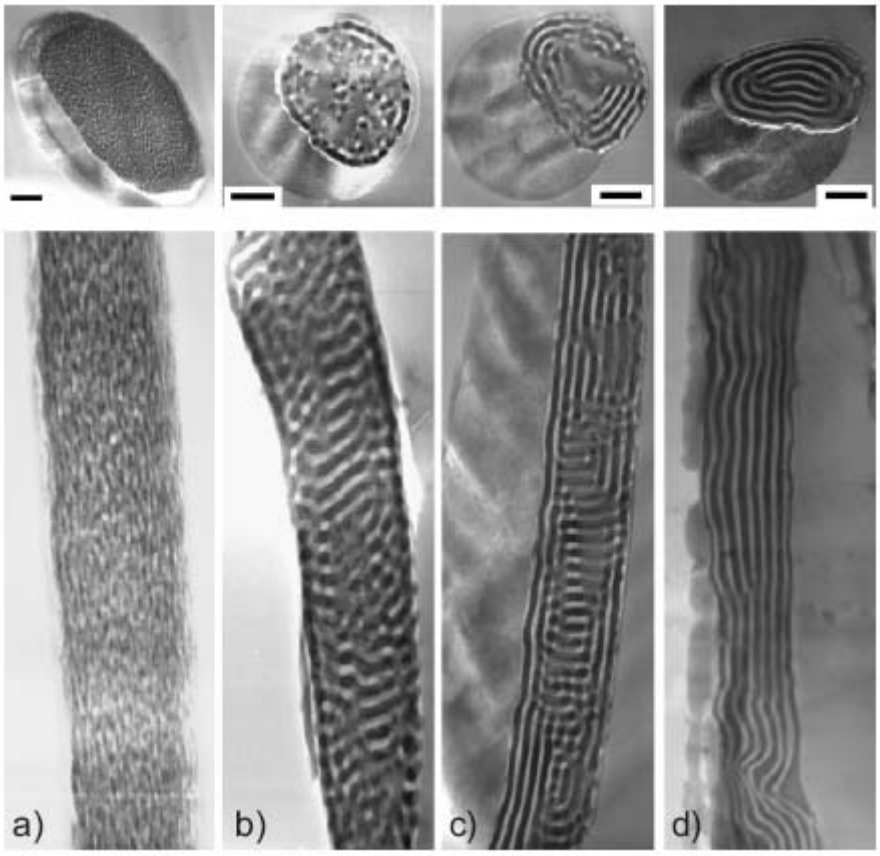

Figure 1.9: TEM images of coaxially spun IS53-143K fibers: a) an as-spun fiber; b) stacked PS lamellar structure after annealing at 125 °C for 24 h; c) transition to alternating concentric-cylinder morphology after annealing at 175 °C for 24 h; and d) parallel morphology on annealing at 175 °C for 50 h. The top row shows the cross sections normal to the fiber axes, and the bottom row shows the cross sections parallel to the fiber axes. The dark areas are stained-PI domains, while the light areas are PS domains. All scale bars are 200 nm [35].

As a follow-up study to the coaxial BCP-silica system, Kalra *et al.* [45] demonstrated the technological application of these self assembled materials by introducing magnetite nanoparticles into the core PS-*b*-PI material. The incorporation of magnetite nanoparticles demonstrated the selectivity and dispersion of such particles into one of the polymer domains in electrospun BCP nanofibers. With the freedom to vary nanoparticle surface coating, block copolymer self-assembly, processing

conditions (e.g. deformation rate) and nanoparticle size, among other parameters, these results demonstrate the possibility of developing an entire spectrum of multifunctional materials with precisely controlled self-assembly (see Figure 1.10).

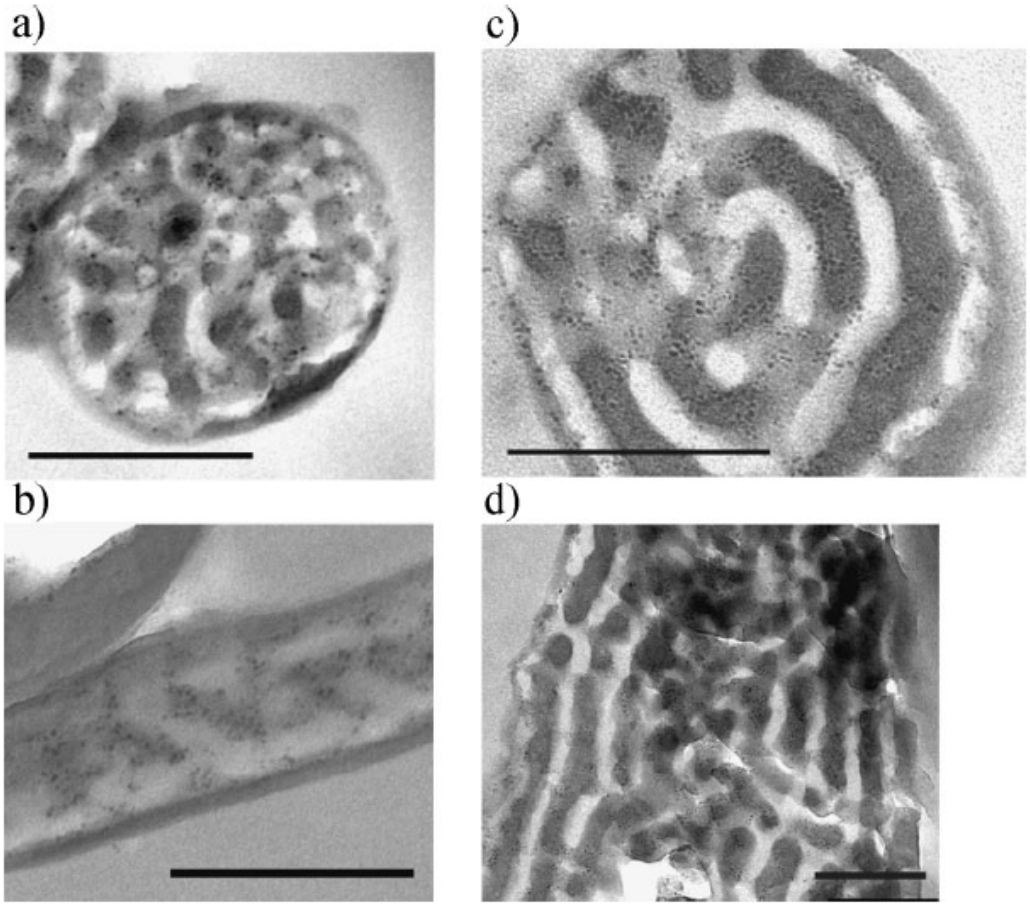

Figure 1.10: TEM images of microtomed coaxial nanofibers with 4 wt% magnetite NP/SI(54-70) as core and silica as shell a) cross sectional cut of fiber, annealed at 125 °C, 24 h, b) fiber cut along the axis, annealed at 125 °C, 24 h, c) cross-sectional cut of fiber, annealed at 175 8C, 50 h, and d) fiber cut along the axis, annealed at 175 °C,50 h. Grey shell region is silica; in the core, light regions are PS domains, dark regions are stained PI domains and even darker dots are magnetite NPs. All scale bars are 200 nm [45].

1.8. Coarse-Grained Molecular Dynamics Simulation

Molecular dynamics(MD) is a form of computer simulation in which atoms and molecules are allowed to interact for a period of time by approximation of known physics, giving a view of the motion of the atoms [46]. It is impossible to keep track of millions of particles and its interactions analytically, and numerical approach is required. It represents an interface between laboratory experiments and theory, and can be understood as virtual experiment.

The basic algorithm of the numerical simulation begins by initilizing position with excluded volume for each particles. Then with a fixed timestep, one can calculate the force between each particles with given potentials, such as Lennard Jones Potential. The positional information can be obtained from the calculated force and acceleration to move the particles. As these steps are repeated for given amount of time intervals, the simulation is completed (see Figure 1.11).

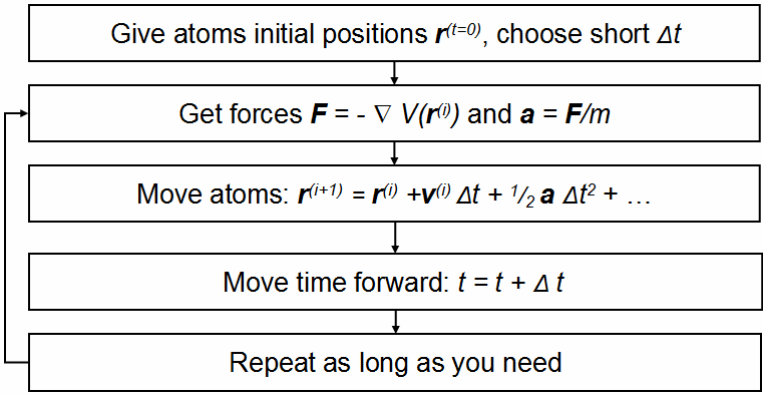

Figure 1.11: Basic algorithm of molecular dynamics

It is computationally expensive to explicitly represent every atom of the complex system, espeically on simulations of process on long timescales(beyond about 1 microsecond). Thus, one can use “psuedo-atoms” to represent groups of atoms by

coarse-graining. For example, "united atom" (sometimes called "extended atom") coarse graining method was used in most early MD simulations of proteins, lipids and nucleic acids. In this method, instead of treating all four atoms of a CH_3 methyl group explicitly (or all three atoms of CH_2 methylene group), one represents the whole group with a single pseudo-atom. This pseudo-atom unit is then properly parameterized so that its Van der Waals interactions with other groups have the proper distance dependence. In case of BCPs, a bead-spring model or a bead-rod model is used as coarse-graining the polymer molecules. In this model, one treats the fixed number of polymer chains as one bead, connected to other beads by a spring with a fixed spring constant, k (see Figure 1.12).

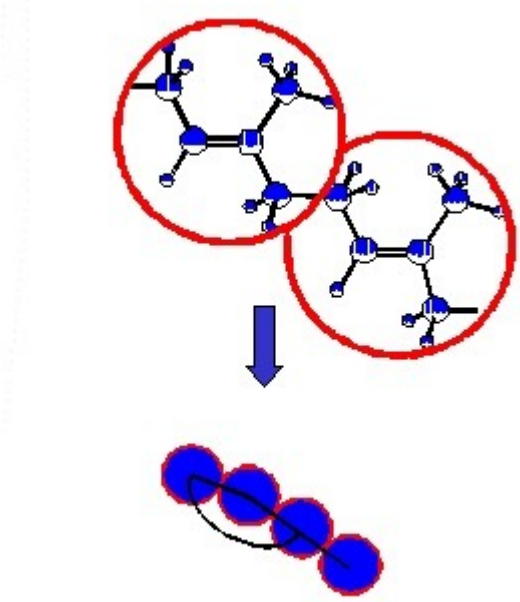

Figure 1.12: Bead-spring model [47]. Instead of representing every single atom, a group of atom is represented as one “bead” connected to next such “bead”. A spring-like potential is connected between the beads

Consideration of potentials is also important in proper MD simulation. Typically, a two-body interaction of Lennard Jones potential with slight modification is used. However, one can also use many-body interactions where the potential energy cannot

be found by a sum over pairs of atoms, as these interactions are calculated explicitly as a combination of higher-order terms.

Kalra *et al.* have MD simulations of BCPs with selective and nonselective nanoparticles under simple shear flow [48]. The result showed that shear can have a significant effect on the location of nanoparticles in BCPs and therefore can be used as another parameter to control nanocomposite self-assembly [48]. If such simulations are taken with elongational flow, followed by relaxation of the flow, then it can compared with its respective results from electrospinning as to gain further insights of the self-assembly of BCPs. Figure 1.13 illustrates results of their molecular dynamics results regarding the effects of shear on the location of selective and nonselective nanoparticles in symmetric BCP [48].

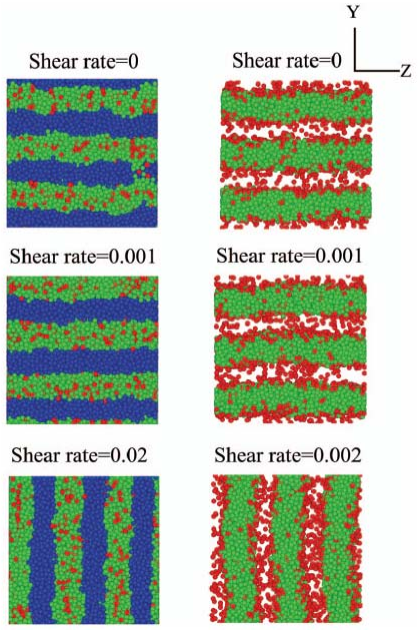

Figure 1.13: Snapshots of nanocomposites with (left) selective NPs at γ=0,0.001 (parallel) and critical shear rate γ =0.02 (perpendicular) and (right) nonselective NPs at ˙=0,0.001 (parallel) and critical shear rate, γ =0.002(perpendicular). Direction of shear is velocity x with y slide. Perpendicular morphologies are shown at respective critical shear rates where a transition from parallel to perpendicular lamellar takes place [48].

1.9. Multi-axial Electrospinning

Recently, there have been a few studies involving tri-axial or multi-axial electrospinning systems. To generate Alcell lignin hollow nanofibers (ALHFs), Lallave *et al.* used a tri-axial configuration of ethanol, lignin, and glycerin(from outermost to innermost layer) where the sheath flow of ethanol was used to avoid solidification of the Taylor cone; while supplying glycerine as a template fluid [49]. Zhao *et al.* [50] have made a biomimmetic system with multi-axial electrospinning. They incorporated multiple inner axial paraffin oil inside $Ti(OiPr)_4$ solution, then removed the organics to create multi layer channel as shown in Figure 1.14.

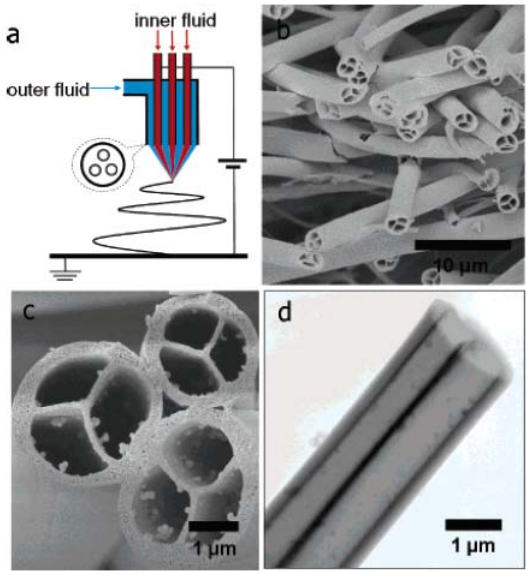

Figure 1.14: (a) Schematic illustration of the three-channel tube fabrication system. The immiscible inner and outer fluids (red for paraffin oil and blue for Ti(O*i*Pr)4 solution) were issued out separately from individual capillaries. (b) Side-view SEM image of sample after the organics have been removed. (c) Magnified SEM image of tubes in which the channels were divided into three independent flabellate parts by a Y-shape inner ridge. (d) TEM image of a three-channel tube [50].

In this paper, a novel tri-axial electrospinning system based on a serial connection of two needles with feeding has been designed and implemented to make silica shell fibers with different combinations of materials for middle and innermost layer. By

adding additional silica layer inside the coaxial silica-BCP system, we sought to confine the polymer domain even further, and study the effect of confinement and wall interaction on self-assembly of BCP both as-spun and annealed. Also, it is possible to dissolve the silica layers using NaOH solution, thus creating hollow BCP nanofibers. This hollow system has a potential to be ultimately used to create more complex biomimmetic system than the aforementioned system by removing one phase of the hollow BCP [50].

In addition, an electrospun system consisting of silica shell as sheath, BCP mixed with homopolymer such as polystyrene in the middle, and silica in the core has been studied to study cylindrical confined dynamics of BCP mixed with homopolymer. Furthermore, functional magnetite nanoparticles coated with oleic acid have been introduced to the BCP domain for aforementioned systems in order to demonstrate the technological applications of these materials.

Finally, these experimental results have been compared with theoretical study by molecular dynamics. In particular, a symmetric model BCP layer sheathed by non-interacting wall in cylindrical confinement has been simulated as to understand the mechanism behind the confinement assembly studied in the tri-axial electrospinning system.

CHAPTER 2

EXPERIMENTAL DESIGN AND SETUP

2.1. Experimental Design

Syringe needles are supplied by Hamilton Company. The needles that are used in the inner two layers of tri-axial setup are combined by molding with fittings that work to separate the layers while taking solution feeds. The needles, when combined, are cut so that the outermost needle is longer than the middle by 0.5 mm, and the middle one longer than the innermost by 0.5 mm. Figure 2.1 shows the combined tri-axial needle setup.

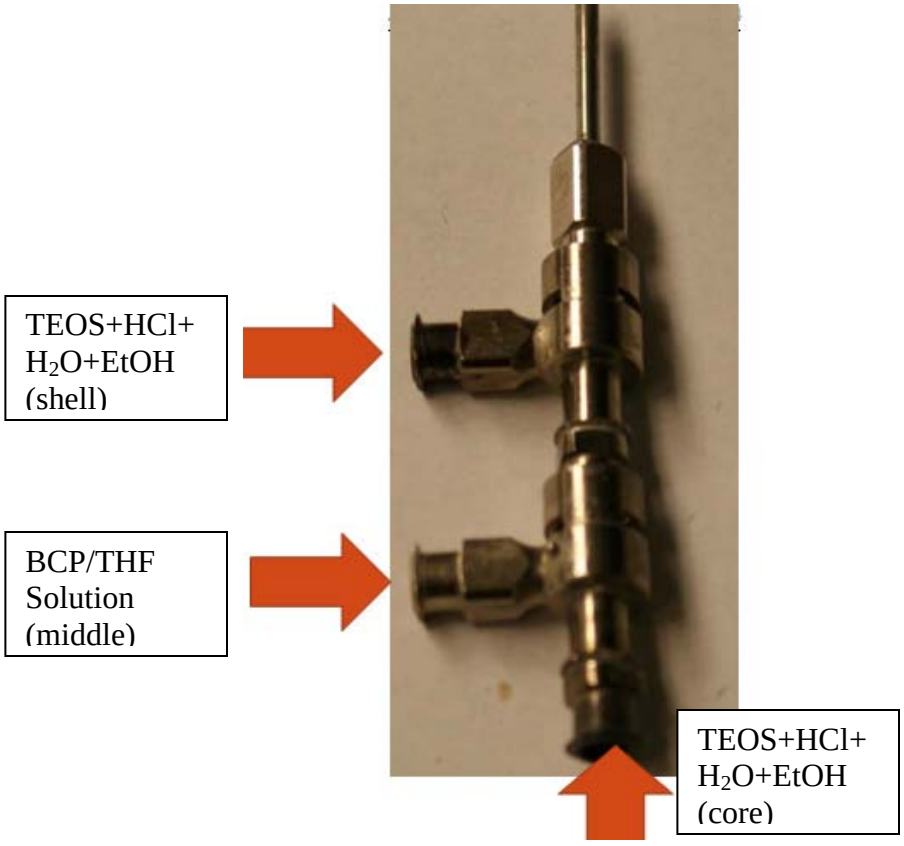

Figure 2.1: The tri-axial electrospinning setup

Originally, the tri-axial needle setup was 30gauge-20gauge-16gauge, which is equivalent to 0.16-0.29-0.28 mm of inner diameters after the three needles are assembled together. However, the electrospun fibers were lacking the core silica when it was examined in Transmission electron microscopy, possibly resulting from clogging of the core needle by viscous silica precursor. The core needle indeed was clogged with silica and often had to be discarded after every trial, greatly reducing the efficiency of experiments. Thus, two more sets of needles with larger diameters 26gauge-18gauge-14gauge (0.26-0.38-0.33 mm) and 22gauge-17gauge-13gauge (0.41-0.35-0.33 mm) were devised. The experimental results shown in subsequent section show that the 22gauge-17gauge-13gauge setup had the most tri-phase nanofibers. Thus this setup was selected to be used for most of the experiments later on. Table 2.1 lists the dimensions of needles used.

Table 2.1: The diameters of the tri-axial needle setup used. Three different kinds of sets were used, in the order of increasing size of overall diameter of combined needle setup from A to C.

Sets		Core	Middle	Shell
A	Needle Gauge(Gauge)	30	20	16
	Inner Diameter(mm)	0.16	0.29	0.28
B	Needle Gauge(Gauge)	26	18	14
	Inner Diameter(mm)	0.26	0.38	0.33
C	Needle Gauge(Gauge)	22	17	13
	Inner Diameter(mm)	0.41	0.35	0.33

It is important to know which variables affect the spinning process the most, and applying the best combination of the variables to optimize the experimental condition. To do so, a qualitative test of electrospinning was done varying viscosity of spinning

material and flow rates. The results from the Table 2.2 a) and b) showed that viscosity is the most important factor to achieve the most favorable electrospinning condition.

Table 2.2: Qualitative analysis of coaxial electrospinning by a) (above) varying silica cooking time(hence, the viscosity) and materials and b) (below) by varying flow rates. - ; no spin, + ; spin with inconsistency, ++ ; good spin with consistency.

a)

Core	Shell	Observation
Si cooked 3 Hrs	Si cooked 5 Hrs	-
Si cooked 4 Hrs	Si cooked 5 Hrs	+
Si cooked 5 Hrs	Si cooked 5 Hrs	+ +
BCP/THF	Si cooked 4 Hrs	+
BCP/THF	Si cooked 5 Hrs	+ +

b)

Core flow(ml/min)	Shell flow(ml/min)	Observation
0.01	0.01	+ +
0.01	0.02	+ +
0.01	0.03	+ +
0.02	0.02	+ +
0.02	0.03	+ +
0.02	0.04	+ +

2.2. Material Synthesis

Tetra(ethyl) ortho silicate (TEOS) was supplied by Aldrich. To produce the sol-gel solution, a molar ratio of TEOS:EtOH: H_2O:HCl of 1:2:2:0.01 was used. Originally, 9.00 g of TEOS and 4.00 g of EtOH are combined, followed by dropwise addition of catalytic solution comprised of 1.56g of H_2O and 3 drops of HCl. The solution is vigorously mixed to produce a homogeneous solution, and placed in a 50^{o}C oven to accelerate the sol-gel reaction. After 5 hours, the solution is ready to be electrospun.

Another scheme of silica precursor was made in order to i) expedite the experimental procedure, and ii) to have enough silica material to be spun. The mass of the material was doubled, while putting the liquid in a beaker with larger surface area for faster reaction (see Figure 2.2). Later in results section we see that the results were improved upon using the new recipe.

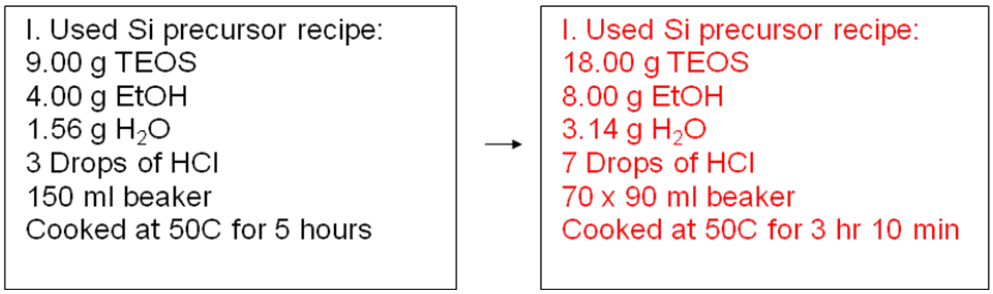

Figure 2.2: a) silica recipe in the initial study on left and b) the improved recipe on right.

PS-*b*-PI block copolymers with MW_{PS} = 53500 g/mol and MW_{PI} = 70000 g/mol were synthesized using a two step living anionic polymerization [30]. *sec*-Butyllithium is used as an initiator to first polymerize styrene monomer anionically and then to initiate isoprene monomer with this living polystyrene to form a living PS-*b*-PI diblock copolymer [30].

Transmission electron microscopy (TEM) and small angle X-ray scattering (SAXS) studies were carried out to show the formation of lamellar/sphere/cylinder morphology in films of the BCPSs cast in THF. Five different PS-*b*-PI polymers were used in this study, with isoprene volume fraction of 0.09, 0.18, 0.28 and 0.74 for asymmetrical composition and 0.53 for symmetrical composition. They are denoted SI-09, SI-19, SI-28, SI-74, and SI-53, respectively, and have total molecular weight of 56200, 50000, 45800, 34100, and 143000 grams, respectively. SI-09 form spheres of the isoprene phase in the bulk, SI-28 and SI-19 form hexagonal cylinders of the isoprene

phase in the bulk while SI-71 forms hexagonal cylinders of the styrene, and SI-53 forms lamellae in accordance with the PS-*b*-PI phase diagram [6], and also as seen in Transmission Electron Microscopy (TEM) studies. The polydispersity of the polymer were measured by gel permeation chromatography and were ~1.04 except for SI-19 which was ~1.40. The details about the aforementioned block copolymer are tabulated in Table 2.3.

Table 2.3: Block copolymers used and their molecular weights, morphologies, and PS fraction

Polymer Name	Molecular Weight(g/mol)	Morphology	PS vol fraction	PDI
SI-09(A22)	56200	PI Sphere	0.09	1.04
SI-19(PIPS2)	45750	PI Sphere	0.19	1.40
SI-28(XXXIII)	45800	PI cylinder	0.28	1.04
SI-53(PIPS7)	143000	Lamellar	0.53	1.04
SI-74(XXX)	34100	PS cylinder	0.74	1.04

The BCPs were dissolved in THF and used magnetic stirrer for about an hour to homogenize the solution. The weight percentage of BCPs in THF was typically in range of 10%~14%, where high molecular weight BCP (approximately 100,000 g/mol) was at 10% and lower molecular weight BCP was typically at 14%.

Monodisperse 4.1±0.55 nm magnetite NPs with oleyl-group surface coating were synthesized using a method similar to the one demonstrated by Sun *et al.* [27] 2 mmol of iron(III) acetylacetonate ($Fe(acac)_3$) was mixed in 20 ml of octadecene with 1,2-hexadecanediol (10 mmol), oleic acid (6 mmol), and oleylamine (6 mmol) under nitrogen and heated to 285 ºC for 30 min (ramping rate: 3 -C minS1). The solution was then allowed to cool to room temperature and excess ethanol was added for

precipitation. The precipitated magnetite NPs were recovered by centrifugation [48]. When magnetic nanoparticles are loaded to BCP/THF solution, the typical weight percentage of nanoparticle is about 5% of the BCP.

The solutions are loaded on plastic syringe and placed on syringe pump provided by Harvard Apparatus. Several ranges of volumetric flow were used per trial, and the most consistent tri-axial nanofibers were made from a combination of 0.02, 0.015, and 0.02 ml/min for core, middle, and shell layer, respectively. An applied voltage of 20 kV was used and the distance from the needle tip to collector was 4.5 inches. The aforementioned spinning conditions were carefully chosen to obtain a continuous production of sub-micron scale fibers through trial and error.

The electropsun fibers were annealed at temperatures in the range of 125^{o}C to 180^{o}C (> BCP glass transition temperature of 100^{o}C) to obtain equilibrium self assembled structures. The annealing was done in a vacuum oven in order to prevent double bond crosslinking from oxidation.

2.3. Characterizations

The as-spun and annealed fibers are embedded using Epofix resin. After 12 hours, the embedded samples are hardened enough to be cut using Leica Ultramicrotome. A diamond knife provided by DiaTome was used on the microtome to slice the samples. The samples were cut in thickness range of 40~80 nm at room temperature (see Figure 2.3).

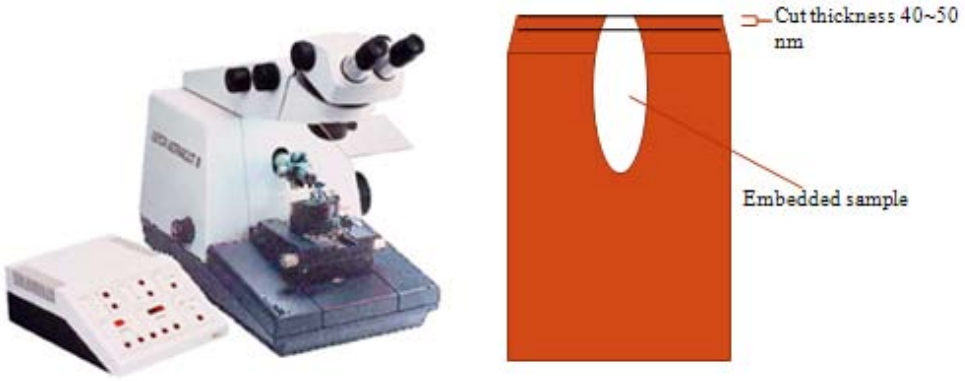

Figure 2.3: Actual image of microtome used (left) and the schematics of microtoming (right)

The microtome sliced the samples along the fiber axis and perpendicular to the axis to view the internal structures. The samples are stained by OsO_4 to differentiate the polyisoprene phase from the polystyrene phase. Transmission electron microscopy (TEM) was conducted using the Tecnai T-12.

CHAPTER 3

EXPERIMENTAL RESULTS

3.1 Early Results and Problems

The tri-axial nanofibers were formed using SI-19 as middle layer, sandwiched by two silica layers. The SI-19 polymer was used as a test material before using other BCPs, for it was the most abundant BCP available in stock, and the most polydisperse polymer among the available BCPs. The initial needle setup used was 30gauge-20gauge-16gauge, with volumetric flow at 0.02-0.02-0.04 ml/min for core, middle, and shell layers, respectively. The TEM image of the tri-axial nanofibers is shown in Figure 3.1.

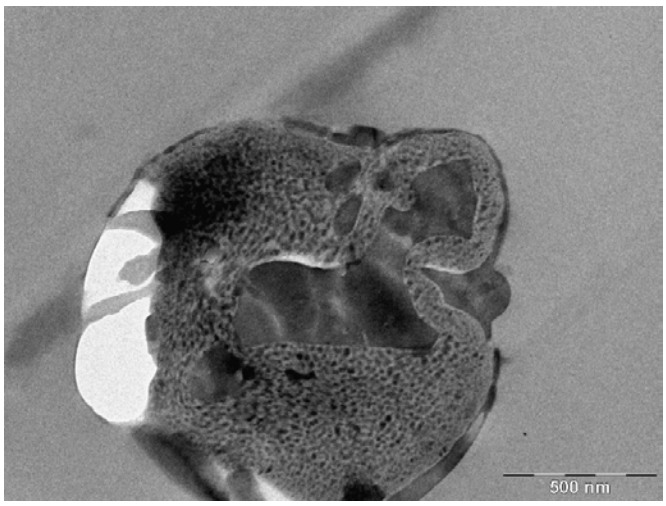

Figure 3.1:TEM image of cross section of as-spun tri-axial nanofiber with SI-19 in the middle sandwiched by two silica layers. Grey shell and core region is silica; in the middle, light regions are PS domains, dark regions are stained PI domains.

As shown in Figure 3.1., the TEM image clearly reveals the BCP layer having both a silica shell layer and a core silica layer embedded in the BCP phase. Few drawbacks

were discovered from this early tri-axial result. This result severely lacked consistency, where less than 1% of the fibers were tri-axial, while majority remained to be a combination of coaxial fibers that lacked the core silica and pure silica nanofibers. Taking complete control of three different layers of solution requires delicate control and attention. In this particular case, the core needle was often found clogged with viscous silica phase towards the end of the electrospinning experiment. The silica precursor was just viscous enough to be electrospun at the beginning of a trial, but as time passed during the experiment, the silica-albeit much slower than in the oven-turns into gel phase. Due to the small diameter of the core needle, the gel silica clogged up, preventing consistent production of the core phase and reducing the efficiency of experiments, for a replacement needle had to be used after every trial.

To improve consistency, a bigger set of needle diameters for core, middle, and shell layers were necessary. Thus, the 26gauge-18gauge-14gauge (core-middle-shell) setup was used. The resulting tri-axial fibers with same combinations of BCPs and silica, along with same volumetric flow rates of 0.02-0.02-0.04(core-middle-shell) ml/min, yielded higher consistency in producing tri-axial nanofibers, which consisted approximately 80% of total nanofibers produced. Figure 3.2 shows TEM images of the resulting fibers.

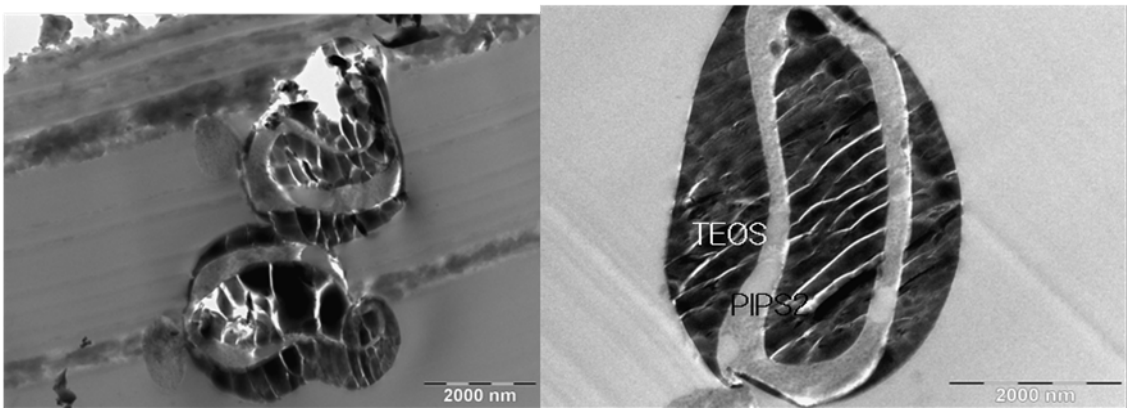

Figure 3.2: TEM images of crosssection of silica-SI-19-silica(core-middle-shell) electrospun fiber using the 26gauge-18gauge-14gauge needle(core-middle-shell) combination. The sample was annealed at 135°C for 7 days.

However, there were a couple problems encountered with this system. First, the fiber diameter is too large to be used for any nano-scale applications, with diameters ranging from 1.5~2.5 micron. Also, the polymer domain size is around 500 nm which is too thick to study any confinement effect on self-assembly of BCP. This may have occurred because i) the needle sizes were bigger, but more importantly ii) the resulting fibers were from the late part of a experimental run, which means the silica precursor solution was more viscous. Higher viscosity results in larger diameters of the electrospun fibers as the fiber diameter D is empirically found to have linear relationship with the solution viscosity, η, i.e. $D = 0.05[\eta]^{0.8}$ [52]. Also, observation from experiments revealed that the polymer jet was not continuously coming out from Taylor cone, especially towards the late stage of the experiment where viscosity became higher. This observation was consistent with the results from TEM as the size distribution of fibers was wide, ranging from 1 micron to 2.5 micron. Nonetheless, the consistent production of tri-axial fiber was greatly improved from 1% to 80%, and

thus this experimental setup was tried with incorporation of other monodisperse BCP, such as SI-53.

The SI-53 replaced SI-19 as the BCP phase sandwiched between two silica layers, while using same conditions as SI-19. As shown in Figure 3.3, the resulting fibers were not tri-axial, missing the silica core inside the polymer. The only difference between SI-53 system and SI-19 system is the polymer itself, implying the material property has affected the result. Indeed, the SI-53 has much higher molecular weight than SI-19, meaning SI-53/THF solution would most likely had higher viscosity than SI-19/THF solution at a given volume fraction of BCP in THF. This trend was also confirmed by other electrospinning experiments [51]. The higher viscosity of SI-53/THF hindered the core silica from properly coming out of the needles, hindering continuous formation of jet. To match the viscosity of SI-53/THF solution with SI-19/THF solution, one can lower the volume fraction of SI-53 in THF from 15% to 10%. The reduction of volume fraction of SI-53(and hence reduction of viscosity) resulted in more consistent production of uniform jet as observed during electrospinning. But the result still did not yield any tri-axial nanofibers.

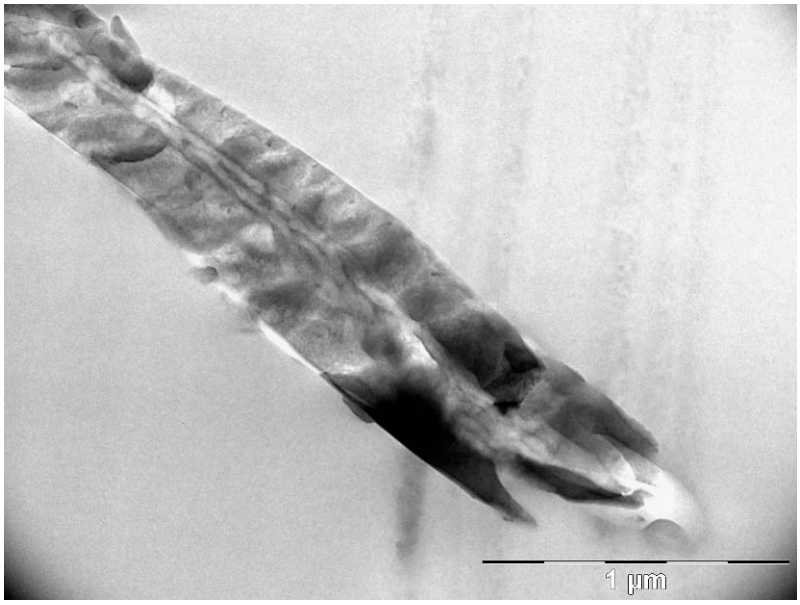

Figure 3.3: TEM image of longitudinal section of SI-53 with silica as shell. This was originally electrospun with silica-SI-53/THF-silica, but the core silica is missing as shown. Annealed at 175 °C for 48hrs.

During experiments, it was found that the core needle gets clogged up by the mixture of silica and the BCP solution. The frequency of clogging in 26 gauge needle was much less compared to the original 30 gauge needle, but this indicated that the core needle size needs to be larger to facilitate consistent core jet fabrication. To eliminate any possibility of clogging in core layer, a larger set of needles with 22gauge-17gauge-13gauge was used for later experiments.

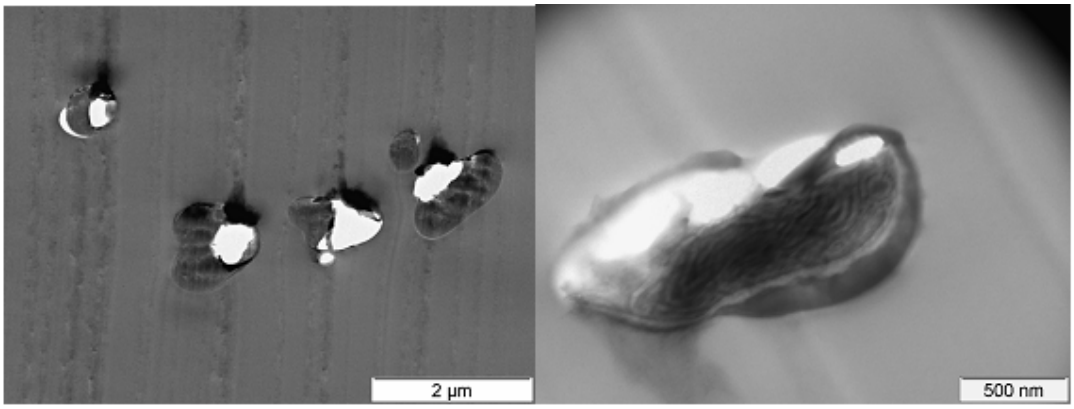

Figure 3.4: TEM images of cross-section of silica-SI-53-silica system. In a) (left) the core layer has been torn out and in b)(right) the shell layer is not properly covering BCP layers

Figure 3.4 shows TEM images of the silica-SI-53–silica (core-middle-shell) system electrospun in 22gauge-17gauge-13gauge needle setup at flow rates 0.02-0.04-0.06 ml/min. In Figure 3.4.a, the core phases of fibers are torn apart. Notably, most of these fibers have diameters in 1~2 micron range. Such deformation most likely came from microtoming, where micron scale fibers were crushed rather than smoothly cutting the cross sections. Indeed, some of the smaller fibers didn't exhibit such deformation (see Figure 3.4.b). But even then it is evident that the fibers didn't form proper tri-axial phases. Figure 3.4. b. shows a fiber with shell silica not properly sheathing the BCP layer.

Three changes were made to improve results. The first change was to use other BCPs with lower molecular weight than SI-53. This change was made since consistent formation of tri-axial fibers could be done with SI-19 whose molecular weight is in similar order of magnitude with the other BCPs except for SI-53. Next, the flow-rates of middle BCP and outer silica shell was lowered to 1) reduce the overall fiber diameter and 2) to avoid forming extensively elongated solution during electrospinning caused by overflow of solution. Some studies suggested that the

volumetric flow rate does affect the size of electrospun fibers [51], and thus decreasing flow rate was expected to reduce the diameter of fibers. Reduction of flow rate also gave us better control over continuous production of fibers, forming ideally shaped Taylor cone more easily. The third change made was to alter the recipe of silica precursor. Up until this point, silica precursor was made using the scheme from Figure 2.2.a). The recipe stated in Figure 2.2 b) not only doubles the amount of silica precursor used, but greatly reduces the gelation time required to reach spinnable viscosity from 5 hours to 3 hours. This was possible since the surface area of the beaker used in Figure 2.2 b) was about 1.5 times bigger than Figure 2.2 a), accelerating the evaporation of EtOH and water from silica precursor. When these three changes were applied to the experiment, the result was greatly improved, as shown in following results.

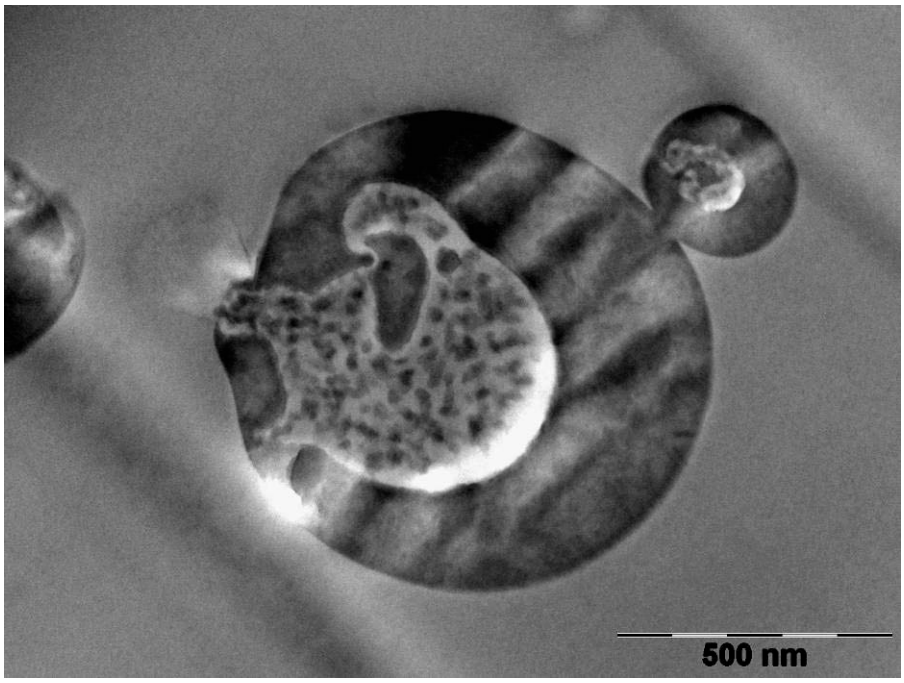

Figure 3.5: TEM image of cross section of SI-09 sandwiched between two silica layers. This was electrospun in 22gauge-17gauge-13gauge with flowrate at 0.02-0.015-0.02 ml/min(core-middle-shell). The sample was annelaed at 150°C for 96 hrs.

Figure 3.5 shows the tri-axial nanofiber that consists of silica-SI-09-silica system. It is evident that the core silica is embedded in the polymer phase, while covered by silica sheath. The tri-axial fibers consisted about 70~80% of total nanofibers, exhibiting consistency of the method. Also, the size diameter ranges from 250 nm~600 nm, staying in submicron scale. Clearly the consistency and size are improved upon using this setup. This experimental setup was used from this point and on.

3.2. Tri-axial Nanofibers with Asymmetrical BCP with NP

The tri-axial nanofibers were electrospun with a block copolymer with magenetite nanoparticle in the middle layer sandwiched between two silica layers. Figure 3.6 shows the TEM images of the cross-section of tri-axial nanofibers using SI-28 as the block copolymer with 5% magnetite nanoparticle loading. We aim to study the self-assembly of block copolymers confined on both sides and the effect of the presence of nanoparticles on the self-assembly. The TEM images evidently show the three layer nanofibers with core and shell silica layers and the BCP with magnetite in the middle layer. The oleic acid coated nanoparticles are selectively present on the isoprene domain of the BCP, serving as both an indicator of isoprene and variable in affecting the confined assembly.

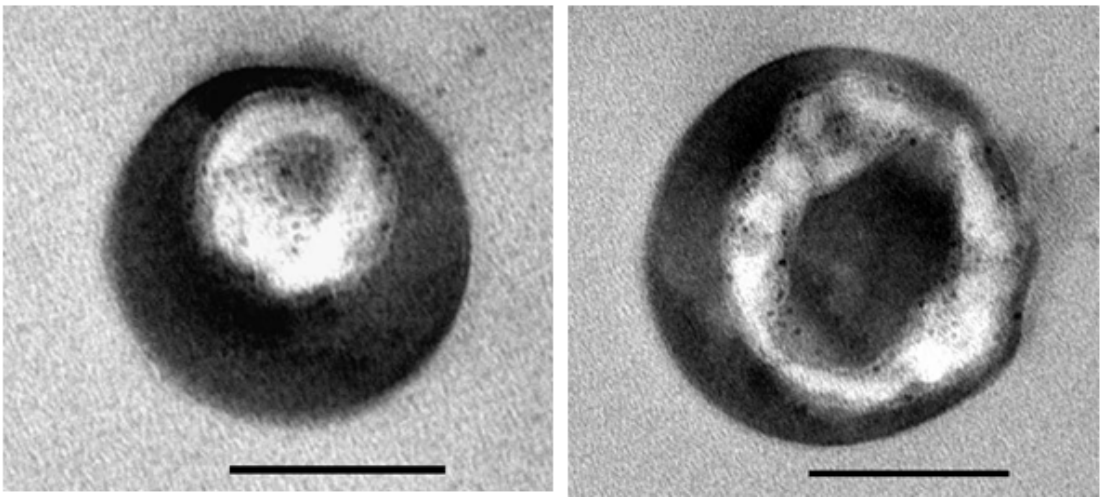

Figure 3.6: (a)(left) and (b)(right) both represent TEM image of cross-section of tri-axial nanofiber with SI-28/magntite NPs sandwiched between two silica layers. The samples are annealed at 150^{o}C for 72 hours. The scale bar is 100 nm.

The thickness of the BCP layer is only about ~ 40 nm, which is comparable to the block copolymer domain size, thus fitting only a single domain of the polymer in the confined space. The interesting thing to note is that the isoprene phase with magnetite shows a preference to the silica walls, and thus most of isoprene and magnetite migrate to both inner and out interfaces with silica. This is opposite to what we observe in the case of pure block copolymers, where styrene shows a preference for the wall [35, 45]. This phenomenon is observed possibly due to the confinement of the polymer phase, or the sandwiched effect of the polymer, or both. This aspect needs to be studied in more detail to truly understand the specific interactions of different blocks with the silica wall and how these interactions change with the presence of nanoparticles. Figure 3.7 shows the comparison between the past coaxial BCP/NP-silica work with the current tri-axial work.

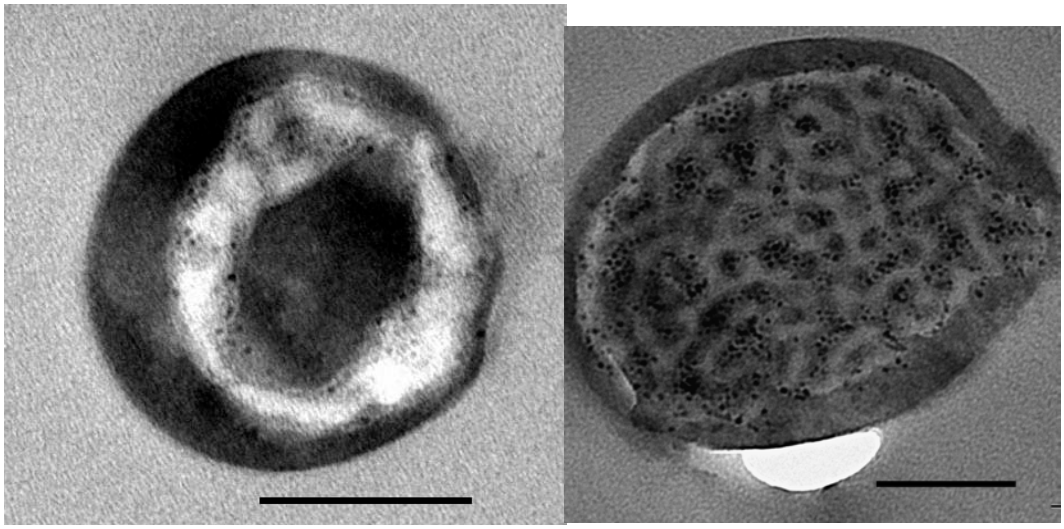

Figure 3.7: Comparison of the tri-axial silica-BCP/NP-silica(on left) with coaxial BCP/NP-silica nanofiber(on right). On left, the black polyisoprene phase exhibits preference toward the silica walls, while on the right the white polystyrene phase shows preference toward the silica wall.

3.3. Tri-axial Nanofibers with Asymmetric BCP with Homopolymer

There have been some studies on the evolution of BCP self-assembly in a homopolymer/BCP blend system. Mareau *et al.* obtained such evolution of BCP self-assembly by blending PS-b-PI with pure polystyrene [53]. By means of slow evaporation (~ 2 weeks, no annealing treatment) after blending the polymers, they were able to see evolution of morphologies from original lamellae to cylinders, gyroids, and sponges. This was possible due to increase in local volume fraction of polystyrene by mixing with pure polystyrene, resulting in localized change of morphology (see Figure 3.8).

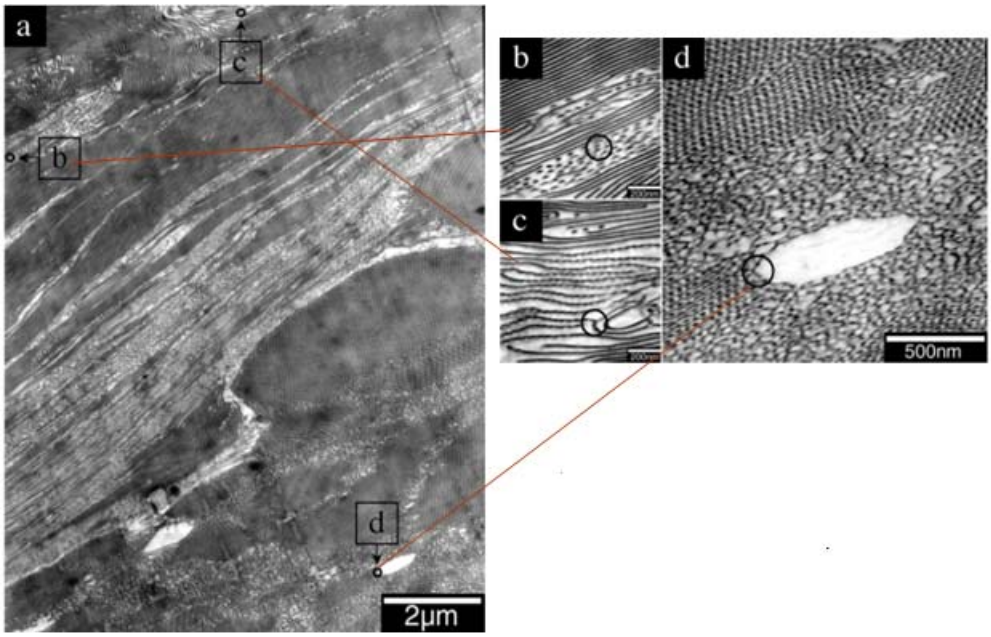

Figure 3.8: TEM images of the 64/36 SI/hS blend, slow evaporation (2weeks). Reference circles (diameter 150 nm) in the main TEM image (a) enable localization of the enlarged areas (b-d). Coexisting morphologies of microphase-separated domains are observed: (b) lamellae, and cylinders; (c) lamellae, cylinders and PL; (d) gyroid,sponge, and hS [53].

Unlike the method presented by Mareau *et al*. [53], electrospinning such BCP/homopolymer blend inevitably involves rapid evaporation during process. It is interesting to discover how the self-assembly of BCP/homopolymer blend would evolve in electrospinning while under i) extreme confinement and ii) sandwiched between two silica walls. PS-*b*-PI block copolymer of PS cylinder morphology (SI-71) was mixed with polystyrene homopolymer (*Mw* = 13,000) (PS-*b*-PI:PS = 65:35), and was placed as the middle layer in tri-axial electrospinning. The ratio of PS-b-PI and PS was chosen so that, by volume fraction of the blended polymer, the polymer would form a lamellae or gyroid structure in equilibrium.

Here, we want to observe if the blend system can evolve into new morphology, while exhibiting the effect of confined assembly seen from the asymmetrical pure BCPs. We also want to see how the presence of PS homopolymer affects the interactions with the silica wall as well. The thermally stable silica shell provides one with opportunity to anneal the materials, thus observing the evolution of the BCP/homopolymer blend structure. Figure 3.9 shows the TEM images of cross section of such fiber sections(annealed at 150^{o}C for 48 hours). As before, the three distinct layers are clearly visible, a BCP/homopolymer blend phase sandwiched between inner and outer silica. The domain size is approximately 40nm, which is a size large enough to be only a single domain size of polymer. The isoprene shows preference to the silica walls, just like the SI-28 tri-axial nanofiber. Again, this is opposite from what we observed from the coaxial pure block copolymer system [35, 45]. The morphology resembles bicontinuous phase, although this is unconfirmed by Small-Angle X-ray Scattering (SAXS) and thus we cannot make any definitive statement about the morphology. Like the asymmetrical pure BCP case, the wall interaction aspect needs to be studied in more detail to obtain better understandings on the specific interactions of different blocks with the silica wall and how these interactions change with the presence of nanoparticles.

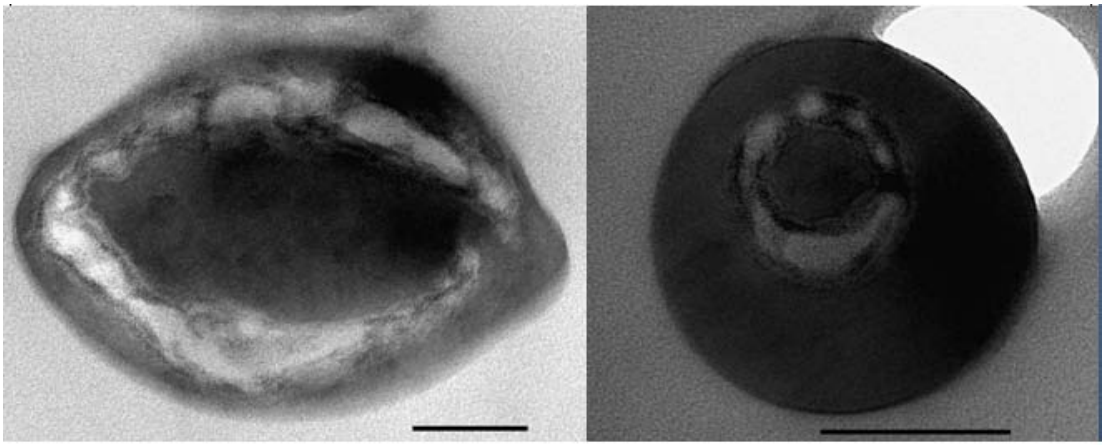

Figure 3.9: TEM images of cross-sections of as-made tri-axial nanofibers SI-71/PS sandwiched between two silica layers. The samples are annealed at 150^{o}C for 48 hours. The scale bars are 100 nm. Again, the PI phase(dark in BCP phase) is wetting against the silica walls.

3.4. Traiaxial Nanofibers with Symmetrical BCP

With successful results coming from BCPs with lower MWs in section 3.2 and 3.3, attention was given to the lamellar forming SI-53 BCP again. The SI-53 BCP was dissolved in THF(13wt%) with silica core/sheath configuration. The same experimental condition used in 3.2 was applied here, and was successful in producing consistent results. Figure 3.9 shows an as-spun longitudinal section of a tri-axial nanofiber(silica-SI-53-silica) and coaxial fiber(SI-53-silica) produced in same set.

As seen from Figure 3.10, the polymer phase is confined in a very small 20nm space. One interesting difference between the coaxial and tri-axial fibers is the morphology of the as-spun BCP. We saw in previous coaxial cases that the BCP morphology was distorted at as-spun state due to the nature of electrospinning [30, 35]. Indeed, the coaxial nanofiber doesn't exhibit any distinct morphology(Figure 3.10 a). However, the tri-axial fiber has lamellar structure preserved, even in as-spun state. The extreme cylindrical confinement of BCP phase could be nullifying the deformational stress

caused by electrospinning, keeping the BCP layer relatively undisturbed. However, this aspect needs further investigation to draw any definitive conclusion.

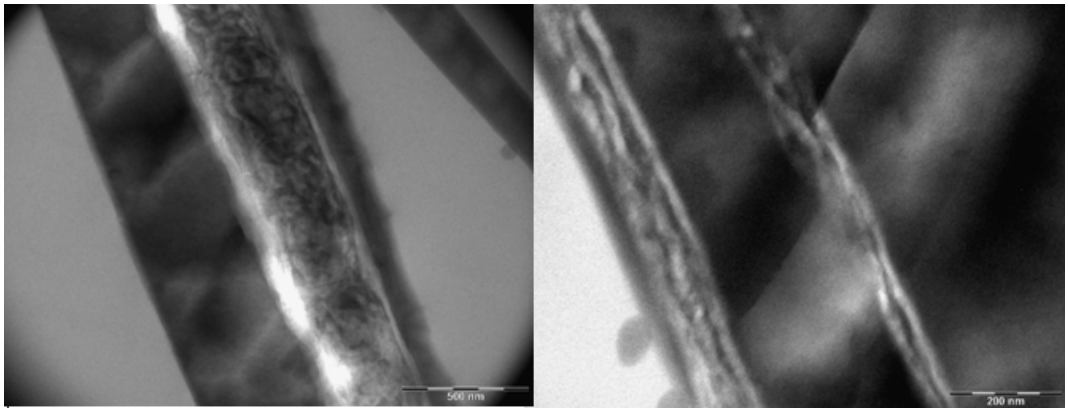

Figure 3.10: TEM images of longitudanal sections of a) SI-53 and silica coaxial nanofiber(left) and b) SI-53 sandwiched between two silica layers(right). a) exhibits disordered morphology, while b) exhibits more ordered, lamellae-like morphology.

Figure 3.11 shows the cross-section of nanofiber annealed at 175°C for 72 hours. Here, the polyisoprene phase shows preference toward the silica wall as seen in all tri-axial nanofibers with polymer domain size smaller than 50nm. We note that the BCP morphology of annealed tri-axial nanofiber exhibits something that resembles a bicontinuous phase. However, we cannot make a definite statement with the image from Figure 3.11, as the confined space is extremely small and the focus of the microscope may not be clear enough to correctly represent the morphology.

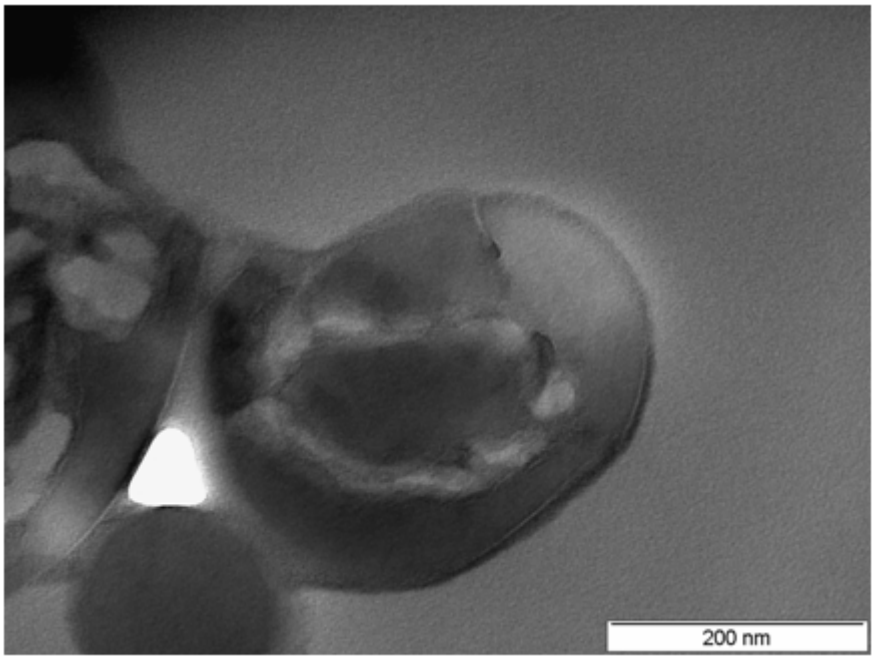

Figure 3.11: TEM image of annealed tri-axial nanofiber(silica-SI-53-silica). The sample was annealed at 175°C for 72 hours.

In order to truly understand what drove such change in morphology, one has to understand whether one polymer phase in BCP has preference towards the wall or not, or if the confinement had kept the BCP from forming other morphology. Molecular dynamics simulation with such consideration would greatly help understand the mechanism of the confined assembly of the block copolymers.

CHAPTER 4

MOLECULAR DYNAMICS SIMULATION

4.1. Models and Potentials

The potentials and parameters were mostly based on the simulation works done by Kalra *et al.* [48]. As stated in Chapter 1.8, the diblock copolymer chains in the current study are modeled as fully flexible bead-spring chains where the monomers are never allowed to overlap. Within a polymer, the neighboring monomers are connected by a finitely extensible nonlinear elastic (FENE) potential,[54]

$$u^{FENE}(r) = -\frac{1}{2} k R_{\max}^2 \ln\left[1 - \left(\frac{r}{R_{\max}}\right)\right], \qquad \textbf{Equation 4.1}$$

where the spring constant k is 30, and the maximum extensibility $R_{\max}$ is 1.5 [54]. The chains consist of A and B blocks of monomers whose excluded volume interactions between them are modeled as a modified purely repulsive Lennard-Jones (LJ) potentials. This modified LJ potential has been cut and shifted to be represented as purely repulsive and is described by,

$$u^{REP}(r) = 4\varepsilon\left[\left(\frac{\sigma}{r}\right)^{12} - \left(\frac{\sigma}{r}\right)^{6}\right] + \varepsilon = u^{LJ}(r) + \varepsilon, r \le 2^{1/6} \qquad \textbf{Equation 4.2}$$

$$u^{REP}(r) = 0, r > 2^{1/6}$$

where r is the separation distance between beads, and σ and ε are the Lennard Jones parameters. This purely repulsive modified LJ potential is often referred to as the Weeks-Chandler-Anderson potential [55].

An attractive potential between like monomers (i.e., *A*-*A* or *B*-*B*) were used to incorporate the physics of microphase separation between the *A* and *B* species. The attractive potential, as described by Horsch *et al.* [56] to model the equilibrium properties of diblock copolymer melts, is again a LJ potential but now it is cut and shifted at values that differ from those presented in Equation 4.2.

$$u^{ATT}(r) = 4\varepsilon\left[\left(\frac{\sigma}{r}\right)^{12} - \left(\frac{\sigma}{r}\right)^{6}\right] - u^{LJ}(2.5), r \le 2.5,$$
$$u^{ATT}(r) = 0, r > 2.5$$

Equation 4.3

The higher cutoff means that this is not purely repulsive and that monomers of the same type are attracted to each other. With this potential, Horsch *et al.* generated various points in the phase diagram, and found good agreement with the phase diagram from mean field theory [48]. They derived the Flory–Huggins χ parameter between the *A* and *B* sites as a function of the simulation temperature [56]. Provided that the temperature is set below the order-disorder transition temperature, the attractive potential taken together with the repulsive *A*-*B* potential ensures that phase separation will occur. In the current study, all simulations were set at a temperature that results in χN value approximately at 50, which is well above the order-disorder transition.

For the nanoparticles, same attractive potential is applied to *A* and *P*, while purely repulsive potential is used between monomer *B* and particle *P* to account for selective NP. The simulation model neglects the effect of nanoparticle rotational dynamics on the rheological behavior of the systems.

4.2. Thermostat

A thermostat that preserves hydrodynamic interaction known as dissipative particle dynamics (DPD) thermostat has been used in the current study. DPD is a simulation technique that was originally conceived to model the interaction of mesoscopic units. The interactions between sites are treated as "soft" potentials meaning that the mesoscopic units can overlap [48]. It was demonstrated by Soddemann *et al.* [57] that this thermostat is effective when using "hard" LJ potentials as is being used in this work [48]. In DPD, we solve the equations of motion,

$$\frac{d\vec{r}}{dt} = \frac{\vec{p}_i}{m_i},$$
$$\frac{d\vec{p}_i}{dt} = \sum_{i \neq j} \vec{F}_{ij}^{C} + \sum_{i \neq j} \vec{F}_{ij}^{D} + \sum_{i \neq j} \vec{F}_{ij}^{R}, \qquad \textbf{Equation 4.4}$$

where $\vec{F}_{ij}^{C}$ is the conservative force that acts between two particles, $\vec{F}_{ij}^{D}$ is a dissipative force and $\vec{F}_{ij}^{R}$ is a random force. The last two terms act as a heat source and drain, thus regulating the simulation cell temperature. The dissipative force $\vec{F}_{ij}^{D}$ can be expressed as

$$\vec{F}_{ij}^{D} = -\xi \omega^{D}(r_{ij})(\vec{v}_{ij} \cdot \hat{r}_{ij})r_{ij}, \qquad \textbf{Equation 4.5}$$

where ξ is a friction parameter and ω^{D} is a weight function. The random force is

$$\vec{F}_{ij}^{R} = \sigma_N \omega^{R}(r_{ij})\xi_{ij}\hat{r}_{ij}, \qquad \textbf{Equation 4.6}$$

where σ_N is a noise parameter and ξ is a white noise variable. By applying the fluctuation-dissipation theorem, the noise parameter σ_N and weight function ω^{D} becomes,

$$\sigma_N = (2k_B T\zeta)^{1/2},$$
$$\omega^D(r) = [\omega^R(r)]^2.$$

Equation 4.7

As reported by Fraser *et al.*,[58] the weight functions used in the current study have the form,

$$\omega^D(r) = \omega^R(r) = \omega(r),$$
$$\omega(r) = \begin{cases} 1, r < r_c \\ 0, r \geq r_c. \end{cases}$$

Equation 4.8

4.3. Computational Details

The chain length of polymer chain length was fixed to ten beads throughout the simulations. The particle volume fraction was fixed at 0.1 for the selective NPs to preserve lamellar morphology in the nanocomposite [59]. The site density ρ was kept fixed at 0.85 and the temperature k_BT was kept at 1.0 [48]. Although the copolymer chain length adopted here is relatively short, it is considered appropriate to capture the essential behavior of symmetric copolymers [60,61] since five beads (approximately five Kuhn lengths) is about the minimum chain length that a block can have to possess oligomeric character (the shortest block in a nonsymmetric copolymer should also be approximately five beads long).

The original cubical system size prior to cylindrical confinement was attained from previous simulation study done by Kalra *et al.* [48]. The cylindrical confinement was built based on this system size. To apply the cylindrical confinement on the diblock copolymer, a fixed cylindrical wall diameter was set in x and y directions. Thus, periodic boundary condition was only applied in z direction (see Figure 4.1). The diameter of wall was set to be approximately 48, which is about 5 times bigger than the polymer domain spacing(~9.1).

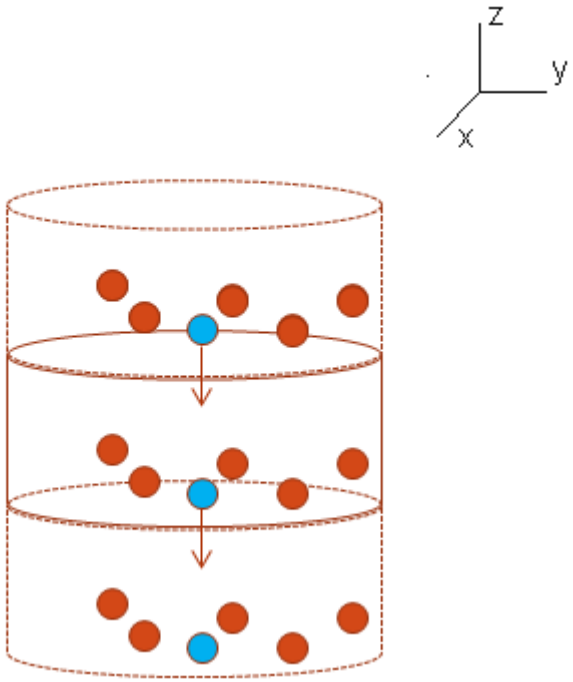

Figure 4.1: Cylindrical confinement imposed on the system with periodic boundary condition applied in z direction.

The velocity Verlet algorithm was used to integrate the equations of motion. The MD integration time step size, Δt, was fixed at 0.01. To make the code efficient, a cell list algorithm was used [62]. The simulations were run for a sufficiently long time until variables such as pressure, potential energy, radius of gyration, and mean squared end-to end distance remained constant. The order parameter O, which is the largest eigenvalue of the Saupe tensor, was studied by Kalra *et al.* with the MD time [48]. O is zero in a completely disordered state and it is unity if the system is perfectly aligned [48]. The parameter was reaching equilibrium when the MD time was approximately 2000 (see Figure 4.2). Since the cylindrical confined BCP simulation essentially used the same parameters except for the confinement of system size, the same number of time steps was used to reach equilibrium.

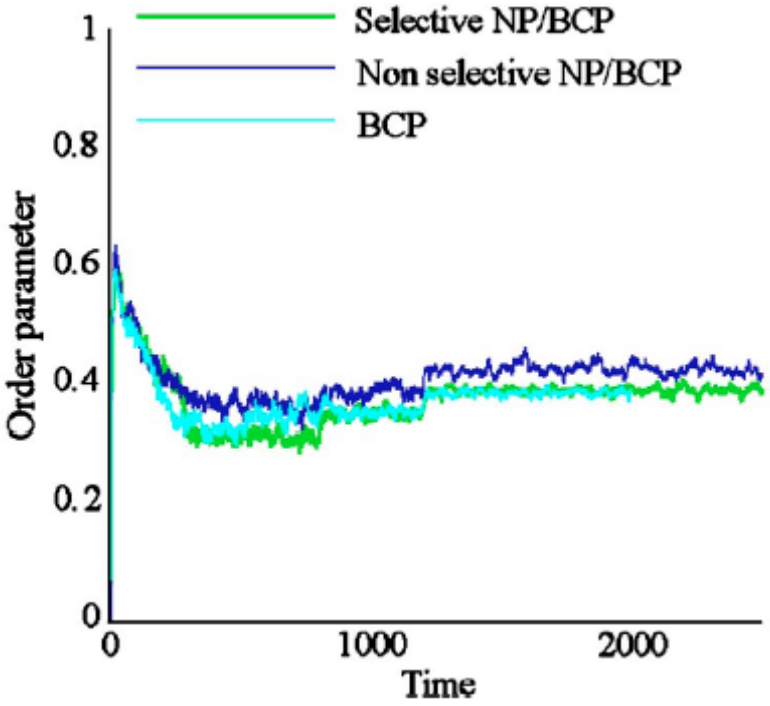

Figure 4.2: Orientation order parameter O as a function of time for selective NP/BCP, nonselective NP/BCP, and pure BCP systems [48].

The NP size used for most part of the current work is same as the size of the Kuhn monomer, and one could then consider such NPs to actually represent a solvent or small oligomer [48]. However, the "NP size/polymer end to end distance" ratio corresponding to such small NPs has been found, in practice, in several instances [63,64]. From our preliminary results, we find that the end-to-end distance of a copolymer chain in the pure block copolymer system used in this work is R_0=4.62, corresponding to σ_p / R_0=0.216, where σ_p (size of NP) =1. Moreover, using the entanglement length as reference, a bead-spring polymer chain with 10 beads would typically represent a molecular weight of ~6 K [54] for a material such as polystyrene, which corresponds to a domain spacing of ~9 nm for a symmetric diblock copolymer or an end-to-end distance of ~4.5 nm [48]. This comparison leads a nanoparticle size of ~1 nm for the simulations, which falls in the nanometer regime. The size of NP

was ensured that the results were not peculiar to the particle size of one Kuhn monomer in previous work, [48] and thus the size of NP was fixed at 1.0. The volume fraction of the NPs, when incorporated, was kept fixed at 0.1 for all systems. The parameters used in this system are summarized in Table 4.1.

Table 4.1: Summary of the MD simulation parameters. The values in MD units are understood to be multiplied by the appropriate combinations of three independent fundamental units of length, mass and energy [62].

Parameters	Symbol	Value(MD units)
Temperature	k_BT	1
Monomer size	σ	1
NP diameter	σ_p	1
NP monomer mass	m	1
Chain length	N	10
Bead density	ρ	0.661
Wall radius	r_{wall}	23.958
Z-axis periodic length	L_z	12.72
Flory-Huggins parameter	χ	53.3
MD integration time step	Δt	0.01
Domain spacing	d	~9.1

4.4. Cylindrical Confinement of BCP Simulation Results

The effect of cylindrical confinement of BCP on self-assembly was studied through coarse-grained MD simulation. The fractions of A and B were both set to 0.5, which is expected to form lamellae morphology at bulk film. This simulation only examined the cylindrical confinement effect without any wall-BCP interaction. As shown in Figure 4.3(simulation results were drawn by Tecplot 10), the simulated result shows that the BCP forms diagonally stacked lamellae morphology.

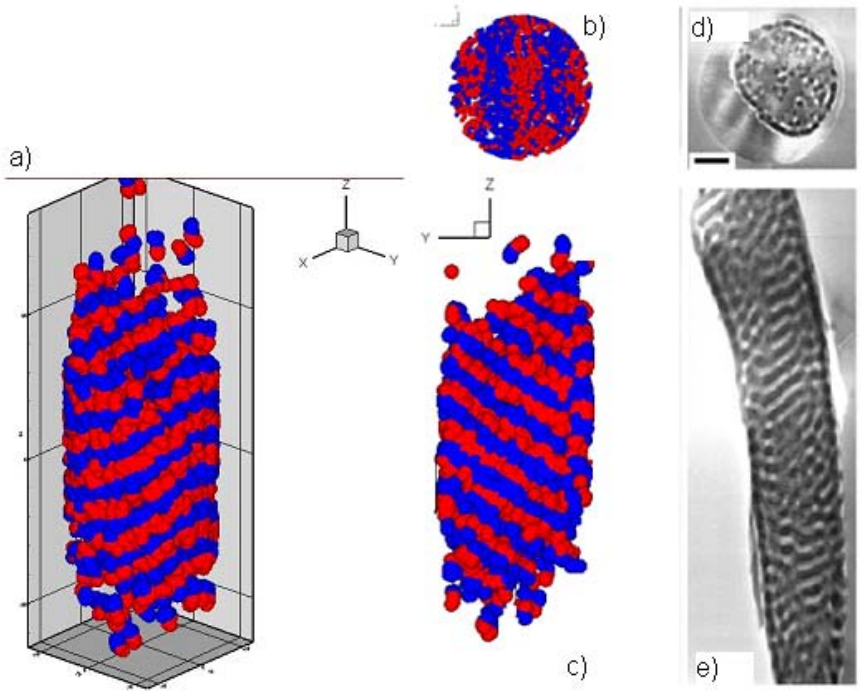

Figure 4.3: MD simulation results of BCP confined in cylindrical wall (in x and y direction). a) shows the 3-D plot results, while b) and c) show the cross-section of a) from the top (cut at z=7) and along the axis (cut at x=0). Red and blue reflect the distinct phases of diblock copolymer. Images d) and e) are the TEM images of experimental results that have similar morphology as b) and c). They are also cross-section from d) top and e) along the axis.

The experimental result with similar morphology was observed in the coaxial electrospun system with symmetric BCP and silica [35]. When the electrospun fiber was annealed at 125°C for 24 hours, the BCP evolved to stacked lamellae (see Figure 4.3 b),c),d),and e) for comparison between simulated result and experimental result). The comparison shows that the simulated result is not unphysical and gives an idea of how it would look in experiments. However, there are two factors that prevent us from direct comparison between the simulation and experimental result. As stated, the MD simulation result was not induced with any shear or elongational flow. But clearly, extreme elongational stress is applied to the nanofiber in electrospinning

experiment and is relaxed during thermal annealing, as seen from previous results [35]. Also, the MD simulation did not take any interaction between wall and BCP into account, while the experimental results showed evidences of one phase segregating towards the silica wall after annealing. We can claim that BCP may prefer to be at stacked lamellae at given cylindrical confinement if wall-BCP interaction is not present. Figure 4.4 shows the comparison of MD simulation result with the cylindrical confinement of symmetric BCP melt from Shin *et al.* [8].

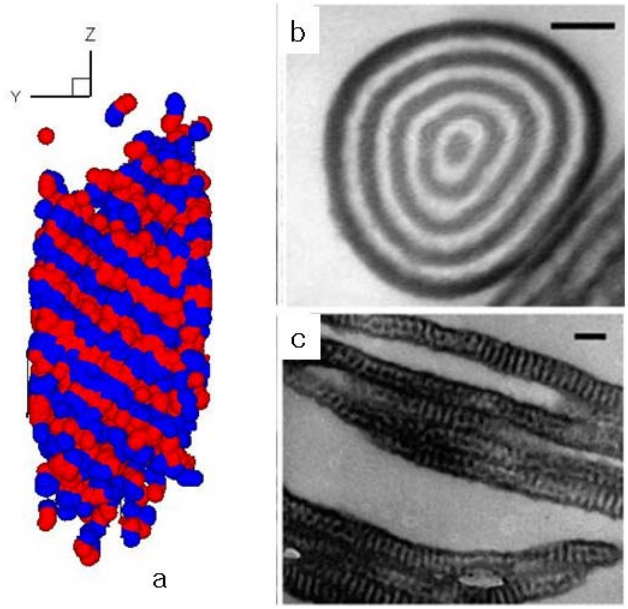

Figure 4.4: The cylindrical confined BCP MD simulation result compared with cylindrically confined melt BCP experimental results [8]. b) formed concentric disk, where one phase of BCP segregated toward the wall. c) shows stacked lamellae for case where the confined diameter was smaller than the domain size of BCP.

The simulation result represents the melt system better than the electorspun system because no shear/elongation is induced on the melt system. Shin *et al.* [8] claimed that when cylindrical confinement diameter is large compared to the equilibrium bulk spacing of BCP, the BCP self-assembles to concentric ring as a result of wall-BCP interaction. When confinement was small compared to BCP domain, it would self-assemble into stacked lamellae. We could implement wall-BCP interaction in

upcoming simulations and compare with the confined melt system to confirm the effect of wall-BCP interaction coupled with that of cylindrical confinement.

4.5. Cylindrical Confinement of BCP/NP Simulation Results

The coarse-grained MD simulation of cylindrically confined BCP/NP system has also been carried out. As stated, the NP volume fraction was set at 10%. The NPs were set to be selective so that it will prefer the blue phase, representing the PI phase of experimental version. As seen from Figure 4.5, the simulated result showed stacked lamellae forming, just as the previous results with pure BCP.

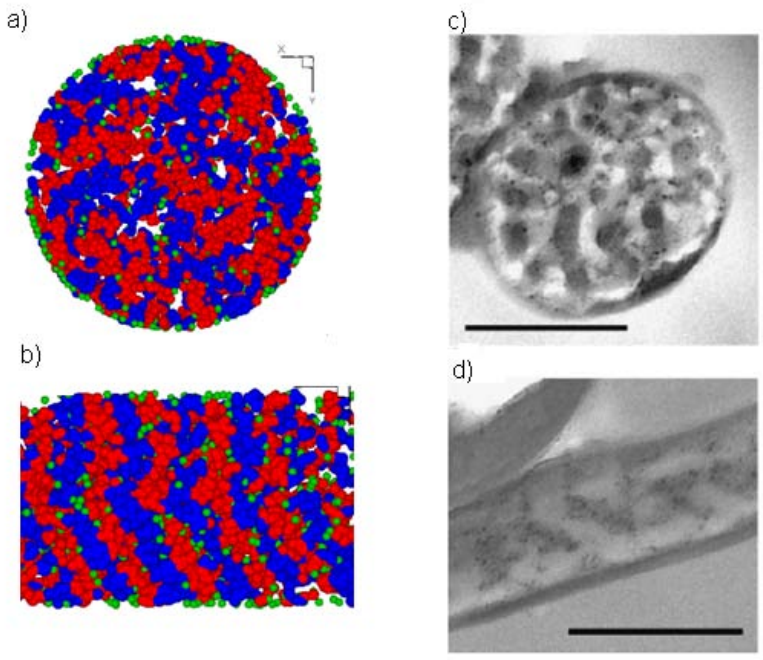

Figure 4.5: MD simulated results of BCP/NP (10% NP) and comparison with experimental result. a) and b) show the cross-section of simulated result from a) the top (cut at z=7) and b) along the axis (cut at x=0). Green represents the nanoparticles with selectivity towards the blue BCP phase. Images c) and d) are the TEM images of experimental results that have similar morphology as a) and b). They are also cross-section from d)top and e) along the axis.

Again, the comparable experimental result was from coaxially electrospun symmetric BCP/NP with silica shell [45]. The same stacked lamellae result was seen when annealed at 125°C for 24 hours. Although the NP percentage was 4% in the experimental case, these results are still comparable as the simulation was implemented with NP volume fraction that was supposed to preserve its originally intended morphology. Again, with no wall interaction taken into account, we can only claim that the stacked lamella morphology is the equilibrium structure if only cylindrical confinement is affecting the BCP self-assembly. Further investigation on these systems is required to confirm and separate the effect of wall-BCP microphase segregation with those of cylindrical confinement on BCP self-assembly. Finally, we note that these nanoparticles with selective interaction towards one of BCP domains tend to migrate towards the wall when they are incorporated into BCP under confinement.

CHAPTER 5

CONCLUSION

A novel electrospinning system that incorporates various BCPs sandwiched between silica walls has been devised, and the effect of confinement and wall interaction on self- assembly of block copolymer nanofibers have been studied. After trial-and-errors of changing intrinsic and process variables, it was found that reducing sol-gel synthesis time, setting flow-rates at order of ~0.02 ml/min, and utilizing larger core size produced the most consistent sub-micron tri-axial fibers.

From the asymmetrical BCP study, it was revealed that the PI phase, rather than PS phase, exhibited preference towards both silica walls. This phenomenon could be a result of extreme cylindrical confinement of the polymer phase, or the sandwiched effect on the polymer, or both. The BCP/homopolymer blend system also exhibited PI preference towards the inner and outer walls. Although the evolution of the morphology resulting from blending seems to be present, further investigation is required. The tri-axial symmetrical BCP system exhibited less distortion of morphology in as-spun state than the coaxial system. The sandwiched extreme confinement effect could be protecting the BCP layer from the elongational stress caused by electrospinning.

Coarse-grained MD simulation has been carried out on cylindrical confinement of symmetric BCP with and without NP inclusion to gain further knowledge on the confinement assembly. The result showed that the BCP exhibits stacked lamellae. This means that the BCP may self-assemble into stacked lamellae if preferential segregation of one microphase towards the wall is not present. The incorporation of

selective NP also yielded same result. Finally, it is predicted that nanoparticles with selective interaction towards one of BCP domains tend to migrate towards the wall when they are incorporated into BCP under confinement.

CHAPTER 6

FUTURE STUDIES

6.1. Experiments

Tri-axial electrospinning of the BCP system have revealed some interesting morphologies and interaction with the walls which are very different from coaxial case. On top of such academically useful findings, we propose to use this system to produce a biomimetic system. It was confirmed by Kalra *et al.* [35] that the silica layer can be dissolved with NaOH. It is also possible to remove one phase of the diblock copolymer to create nanoporous BCP. Chen *et al.* [65] removed the PI phase from PS-b-PI/PS blend system by ozonolysis. They found that their method could remove 70%, 80% and 90% of PI domains for morphologies with PI hexagonal cylinders, PI gyroids, and PI lamellae, respectively. We first propose to transform the tri-axial nanofibers into hollow BCP nanofiber by dissolving the silica shell and core with NaOH. Then, using methods by Chen *et al.* [65], we propose to make nanoporous BCPs. These experiments are ready to be implemented as we already possess the tri-axial nanofibers with the morphologies tested by Chen *et al.* [65] The set of aforementioned methods can yield a multi-channeled hollow tube that also has ability to create tubes from inner layer to outer layer of BCP (see Figure 6.1). This nanostructure has more advanced functional structure than the biommetic system electrospun by Zhao *et al.* [50], as our system allow possible radial transport. Our system also only requires three axes in total regardless of the number of tubes desired, whereas the method by Zhao *et al.* [50] requires the corresponding number of axes to the make the corresponding number of channels. The resulting multi-structured nanofibers may be developed for high end applications such as drug delivery.

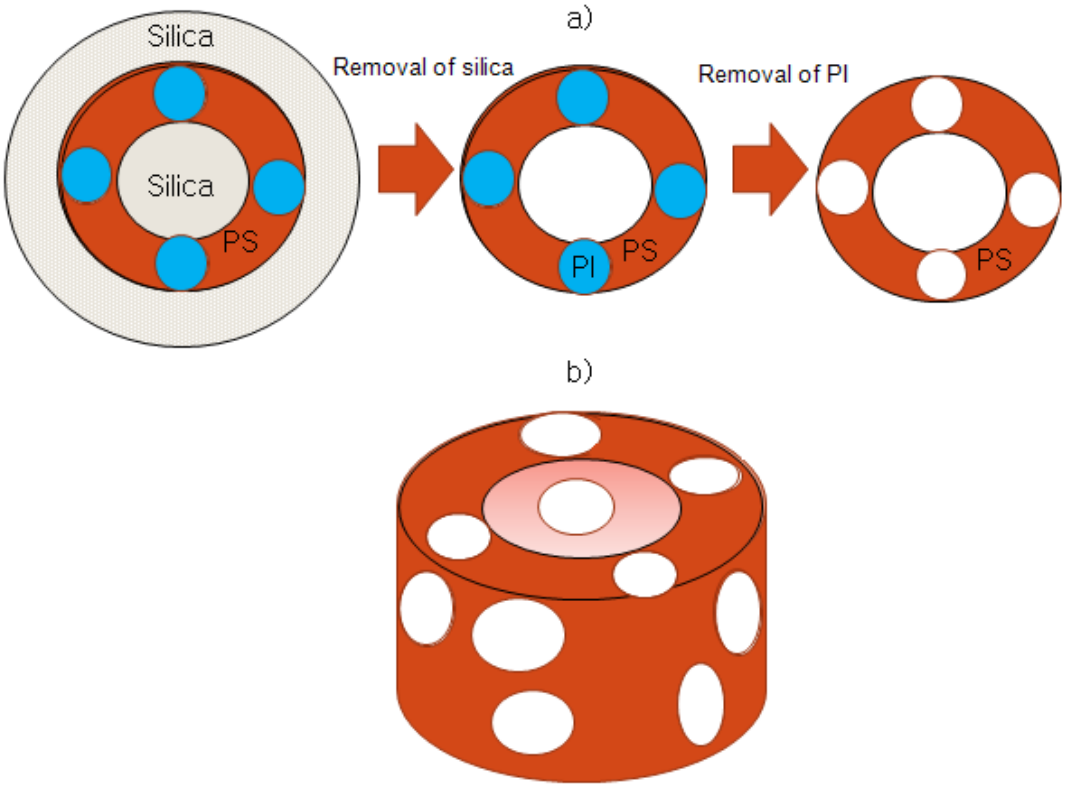

Figure 6.1: Schematic of multi-channeled nanofiber fabrication. The fabrication process is shown in 2-D in a) (above), and b) (below) shows the 3-D picture of the projected outcome.

Also, we propose to do further research on the tri-axial electrospinning by incorporating other intrinsic variables. We could see the effect of molecular weight on NP dispersion by electrospinning two lamellae-forming BCPs with high molecular weight and low molecular weight. It was observed from MD simulation that when lamellae BCP chain length was shortened, the selective NPs were dispersed along the center of BCP microdomains. The previous results with electrospun BCP/NP system did not exhibit such dispersion [45]. By incorporating the selective NPs into BCP with lower molecular weight (by a factor of ~ 1/5), we'll be able to observe the similar result as simulation. This could also be done by using NPs with different sizes as well. This will confirm the effect of relative chain length compared to NP on dispersion of

these particles. By doing this with tri-axial electrospinning setup, one can also examine the effect of confined assembly and wall-interaction.

Finally, we will try electrospinning more advanced BCPs such as graft polymers. We would like to examine the evolution of graft polymers morphology by confinement and its wall interaction by tri-axial and coaxial electrospinning with silica precursor.

6.2. Coarse-grained MD Simulations

Cylindrical confinement effect of BCP was found using coarse-grained MD simulation. First, we propose to reenact the BCP preferential segregation towards wall by applying attractive potential on one phase of BCP while applying repulsive potential on the other phase. If the result yields concentric ring as shown by Shin *et al.* [8], this will confirm the presence of independent effect of wall-BCP interaction, apart from the cylindrical confinement effect. If the result yields stacked lamellae, it may mean either that the independent wall-BCP interaction is not present, or more likely, the confinement effect was overpowering the wall-BCP interaction. We can also try changing diameter of confinement wall to see how the self-assembly of BCP evolves by degree of confinement.

We also propose to apply flow dynamics and relaxation to the cylindrical confinement simulation. By applying elongation, one can truly emulate the dynamics of electrospun BCPs. Then, we propose to compare the annealing process done in experiments with the relaxation of elongational stress done on MD simulation. Annealing is essentially a relaxation of deformational stress done on BCP, and by emulating such relaxation in MD simulation, one can gain further insights of confined self-assembly in electrospinning.

And ultimately, we can also impose the extra wall layer inside the BCP and compare the results with tri-axial silica/BCP/silica experimental results. By studying the sandwiched confinement effect of BCP in various wall diameters, we can gain better understanding of the self-assembly mechanism in multilayered nanofibers.

REFERENCES

1. Bates, F. S. and Fredrickson, G. H. “Block Copolymer Thermodynamics: Theory and Experiment”, *Annu. Rev. Phys. Chem*. **41**, 525 (1990)
2. Szwarc, M., Levy, M. and Milkovich, R. “Polymerization Initiated by Electron transfer to Monomer. A New Method of Formation of Block Polymers”, *J. Am. Chem. Soc*. **78**, 2656 (1956)
3. Schlick, S. and Levy, M. “Block-polymers of Styrene and Isoprene with Variable Distribution of Monomers along the Polymeric Chain. Synthesis and Properties”, *J. Phys. Chem.* **64**, 883 (1960)
4. Boor, J. “Ziegler-Natta Catalysts and Polymerizations”, *Academic Press*, 1979, New York.
5. Morgan, P. W. “Condensation Polymers: by Interfacial and Solution Methods”, *Interscience Publishers*, 1965, New York.
6. Khandpur, A. K., Forster, S., Bates, F. S., Hamley, I. W., Ryan, A. J., Bras, W., Almdal, K. and Mortensem, K. “Polyisoprene-polystyrene Diblock Copolymer Phase Diagram near the Order-disorder Transition”, *Macromolecules* **28**, 8796 **(**1995)
7. Jiang, Z.B., Wang R. and Xue G., “Self-assembly of ABC Triblock Copolymer Thin Films on a Brush-coated Substrate”, *Chinese J. Polym. Sci*. **27**,583 (2009)
8. Shin, K., Xiang, H., Moon, S. I., Kim, T., McCarthy, T. J. and Russell, T. P. “Curving and frustrating flatland”, *Science* **306**, 76 (2004)
9. Xiang, H. Shin, K. Kim, T. Moon, S. I. McCarthy, T. J. and Russell, T. P. “Block Copolymers under Cylindrical Confinement”, *Macromolecules* **37**, 15, 5660 (2004**)**

10. Wu, Y., Cheng, G., Katsov, K.,Sides, S. W., Wang, J., Tang, J., Fredrickson, G. H., Moskovits, M. and Stucky, G. D. “Composite Mesostructures by Nano-confinement”, *Nat. Mater.* **3**, 816 (2004)
11. Warren, S. C., Messina, L. C., Slaughter, L. S., Kamperman, M., Zhou, Q., Gruner, S. M., DiSalvo, F. J. and Wiesner, U. “Ordered Mesoporous Materials from Metal Nanoparticle-block Copolymer Self-assembly”, *Science* **320**, 1748 **(**2008)
12. Balazs, A. C., Emrick, T. and Russell, T. P. “Nanoparticle-polymer Composites: Where Two Small Worlds Meet” *Science* **314**, 1107 (2006)
13. Bockstaller, M. R., Mickiewicz, R. A. and Thomas, E. L. "Block Copolymer Nanocomposites: Perspectives for Tailored Functional Materials", *Adv. Mater.* **17**, 1331. (2005)
14. Chiu, J. J., Kim, B.J., Kramer, E. J. and Pine, D. J. “Control of Nanoparticle Location in Block Copolymers”, *J. Am. Chem. Soc*. **127**, 5036 (2005)
15. Schultz, A. J., Hall, C. K. and Genzer, J. “Computer Simulation of Block Copolymer/nanoparticle Composites”, *Macromolecules* **38**, 3007 (2005)
16. Warren, S. C., DiSalvo, F. J. and Wiesner, U. “Naonoparticle-tuned Assembly and Disassembly of Mesostructured Silica Hybrids”, *Nat. Mater.* **6**, 156 (2007)
17. Sides, S. W., Kim, B. J., Kramer, E. J. and Fredrickson, G. H. “Hybrid Particle-field Simulations of Polymer Nanocomposites”, *Phys. Rev. Lett*. **96**, 250601. (2006)
18. Harris, L. A., Goff, J. D., Carmichael, A. Y., Riffle, J. S., Harburn, J. J., St. Pierre, T. G. and Saunders, M. “Magnetite Nanoparticle Dispersions Stabilized with Triblock Copolymers”, *Chem. Mater.* **15**, 1367 (2003)

19. Park, M. J. and Char, K. “Effect of the Casting Solvent on the Morphology of Poly(styrene-b-isoprene) Diblock Copolymer/Magnetic Nanoparticle Mixtures”, *Langmuir* **22**, 1375 (2006)
20. Jeong, U., Teng, X., Wang, Y., Yang, H. and Xia, Y. “Superparamagnetic Colloids: Controlled Synthesis and Niche Applications”, *Adv. Mater.* **19**, 33 (2007)
21. Park, J., An, K., Hwang, Y., Park, J. G., Noh, H. J., Kim, J. Y. Park, J. H., Hwang, N. M. and Hyeon, T. “Ultra-large-scale Syntheses of Monodisperse Nanocrystals”, *Nat. Mater.* **3**, 891 (2003)
22. Yarin, A. L., Koombhongse, S., Reneker, D. H. “Taylor cone and jetting from liquid droplets in electrospinning of nanofibers” *Journal of Applied Physics* **90**, 4836-46 (2001**)**
23. Kalra, V., Lee, J. H., Park, J. Marquez, M. and Joo, Y. L."Confined Assembly of Asymmetric Block Copolymer Nanofibers via Multi-axial Jet Electrospinning", *Small (in press, 2009)*
24. Fong, H. and Reneker, D. H. “6. Electrospinning and the Formation of Nanofibers.” *Structure Formation in Polymeric Fibers.* 2001, D.R. Salem, Hanser Gardner Publications.
25. Li, D. and Xia, Y. “Electrospinning of Nanofibers: Reinventing the Wheel?” *Adv. Mater.* **16**, 1151 (2004)
26. Klein, L. C. “Part III Continuous, Discontinuous, and Woven Fibers.” *Sol-Gel technology for thin films, fibers, performs, electronics, and specialty shapes.* 1988.
27. Fong, H. and Reneker, D. H. “Elastomeric Nanofibers of Styrene-butadiene-styrene Triblock Copolymer”, *J. Polym. Sci. Part B* **37**, 3488 (1999)

28. Ma, M., Hill, R. M., Lowery, J. L., Fridrikh, S. V. and Rutledge, G. C. "Electrospun poly(styrene-block-dimethylsiloxane) block copolymer fibers exhibiting superhydrophobicity" *Langmuir* **21**, 5549 (2005)
29. Ruotsalainen, T., Turku, J., Heikkila, P., Ruokolainen, J., Nykanen, A., Laitinen, T., Torkkeli, M., Serimaa, R., ten Brink, G., Harlin, A. and Ikkala, O. "Towards Internal Structuring of Electrospun Fibers by Hierarchical Self-assembly of Polymeric Comb-shaped Supramolecules" *Ad*v. *Mater.* **17**, 1048 (2005)
30. Kalra, V., Kakad, P. A., Mendez, S., Ivannikov, T. Kamperman, M. and Joo, Y. L. "Self-Assembled Structures in Electrospun Poly(styrene-block-isoprene) Fibers", *Macromolecules* **39**, 5453 (2006)
31. Seguela, R. and Homme, J. P. "Deformation Mechanism of Thermoplastic 2-phase Elastomers of Lamellar Morphology Having a High Volume Fraction of Rubbery Microphase", *Macromolecules* **14**, 197 (1981)
32. Daniel, C., Hamley, I. W., Mortensen, K. "Effect of Planar Extension on the Structure and Mechanical Properties of Polystyrene-poly(ethylene-co-butylene)-polystyrene Triblock Copolymers", *Polymer*, **41**, 9239 (2000)
33. Pakula, T., Saijo, K., Kawai, H., Hashimoto, T. "Deformation-behavior of Styrene Butadiene Styrene Triblock Copolymer with Cylindrical Morphology", *Macromolecules*, **18**, 1294 (1985)
34. Kim, G. and Libera, M. "Morphological Development in Solvent-cast Polystyrene-polybutadiene-polystyrene (SBS) Triblock Copolymer Thin Films", *Macromolecules*, **31**, 2569. **(**1998)
35. Kalra, V., Mendez, S., Lee, J. H., Nguyen, H., Marquez, M. and Joo, Y. L. ``Confined Assembly in Coaxially Electrospun Block-Copolymer Fibers", *Adv. Mater*. **18**, 3299 (2006)

36. Panels, J. E. “Fuctionalization of Silica Nanofiber Mats via Electrospinning/Sol-gel Synthesis”, M.S. Thesis, Cornell University. (2006)
37. Klein, L. C. “Part I Chemistry and Phase Transformations.” *Sol-Gel technology for thin films, fibers, performs, electronics, and specialty shapes.* 1988.
38. Rao, A. V. and Bhagat, S. D. ” Synthesis and Physical Properties of TEOS-based Silica Aerogels Prepared by Two Step (acid–base) Sol–gel Process” *Solid State Sciences* **6**, 945 (2004)
39. Choi, S. S., Lee, S. G., Im, S. S., Kim, S. H., Joo, Y. L. “Silica Nanofibers from Electrospinning/Sol-gel Process.” *J. Mat. Sci. Letters.* **22**, 891 (2003)
40. Huang, Z. M., Zhang, Y. Z., Kotaki, M., Ramakrishna, S. “A Review on Polymer Nanofibers by Electrospinning and their Applications in Nanocomposites.” *Compos. Sci. Technol.* **63**, 2223 (2003)
41. Carotta, M.C., Ferroni, M., Gherardi, S., Guidi, V., Malagu, C., Martinelli, G., Sacerdoti, M., Di Vona, M. L., Licoccia, S., Traversa, E. “Thick-film Gas Sensors based on Vanadium-Titanium Oxide Powders prepared by Sol-gel Synthesis” *Journal of the European Ceramic Society* **24**, 1409 (2004)
42. Zhuiykov, S., Wlodarski, W., Li, Y. “Nanocrystalline V_2O_5-TiO_2 Thin-films for Oxygen Sensing Prepared by Sol-gel Process” *Sensors and Actuators B-Chemical* **77**, 484 (2001)
43. Sun, Z. C., Zussman, E., Yarin, A. L., Wendorff, J. H., Greiner, A. “Compound Core-shell Polymer Nanofibers by Co-electrospinning” *Adv. Mater*. **15**, 1929 (2003)
44. Yu, J. H., Fridrikh, S. V., Rutledge, G. C. “Production of Submicrometer Diameter Fibers by Two-fluid Electrospinning “ *Adv. Mater.* **16**, 1562 (2004)

45. Kalra, V., Lee, J., Lee, J. H., Lee, S. G., Marquez, M., Wiesner, U. and Joo, Y. L. "Controlling Nanoparticle Location via Confined Assembly in Electrospun Block Copolymer Nanofibers", *Small* **4**, 2067 (2008)

46. Alder, B.J. and Wainwright, T.E., "Studies in Molecular Dynamics. I. General Method" *J. Chem. Phys.* **31**, 459 (1959)

47. Milano, G. and Müller-Plathe, F. "Mapping Atomistic Simulations to Mesoscopic Models: A Systematic Coarse-Graining Procedure for Vinyl Polymer Chains**"** *J. Phys. Chem. B.* **109**, 18609 (2005)

48. Kalra, V., Mendez, S., Escobedo, F. and Joo, Y. L. "Coarse-grained Molecular Dynamics Simulation on the Placement of Nanoparticles within Symmetric Diblock Copolymers under Shear flow", *J. Chem. Phys.* **128**, 164909 (2008)

49. Lallave, M., Bedia, M. J., Ruiz-Rosas, R., Rodriguez-Mirasol, J., Cordero, T., Otero, J. C., Marques, M., Barrero, A. and Loscertales, I. G. "Filled and Hollow Carbon Nanofibers by Coaxial Electrospinning of Alcell Lignin without Binder Polymers", *Adv. Mater.* **19**, 4292 (2007)

50. Zhao, Y., Cao, X. Y. and Jiang, L. "Bio-mimic Multichannel Microtubes by a Facile Method", *J. Am. Chem. Soc.* **129**, 764 (2007)

51. Tan, S. H., Inai, R., Kotaki, M. and Ramakrishna, S. "Systematic Parameter Sutyd for Ultra-fine Fiber Fabrication via Electrospinning Process", *Polymer* **46,** 6128 (2005)

52. McKee, M.G., Wilkes, G. L., Colby, R. H. and Long, T. E. **"**Correlations of Solution Rheology with Electrospun Fiber Formation of Linear and Branched Polyesters" *Macromolecules* **37**, 1760 (2004)

53. Mareau, V. H., Matsushita, T., Nakamura, E. and Hasegawa, H. "Growth of Gyroid Grains in the Complex Phase Window of PS-*b*-PI/PS Blends" *Macromolecules* **40**, 6916 (2007)

54. Kremer, K. and Grest, G. S. “Dynamics of entangled linear polymer melts: A molecular-dynamics simulation” *J. Chem. Phys*. **92**, 5057 (1990)

55. Weeks, J. D., Chandler, D. and Anderson, H. C. “Role of Repulsive Forces in Determining the Equilibrium Structure of Simple Liquids” *J. Chem. Phys.* **54**, 5237 (1971)

56. Horsch, M. A., Zhang, Z., Iacovella, C. R. and Glotzer, S. C. “Hydrodynamics and microphase ordering in block copolymers: Are hydrodynamics required for ordered phases with periodicity in more than one dimension?”*J. Chem.Phys*. **121**, 11455 (2004).

57. Soddemann, T., Dunweg, B. and Kremer, K. “Dissipative particle dynamics: A useful thermostat for equilibrium and nonequilibrium molecular dynamics simulations” *Phys. Rev. E* **68**, 046702 (2003)

58. Fraser, B., Denniston, C. and Muser, M. H. “On the orientation of lamellar block copolymer phases under shear” *J. Chem. Phys*. **124**, 104902 (2006)

59. Schultz, A. J., Hall, C. K. and Genzer, J. “Computer Simulation of Block Copolymer/Nanoparticle Composites” *Macromolecules* **38**, 3007 (2005)

60. Fraser, B., Denniston, C. and Muser, M. H. “Diffusion, elasticity, and shear flow in self-assembled block copolymers: A molecular dynamics study” *J. Polym. Sci. Part B: Polym.Phys.* **43**, 970 (2005)

61. Murat, M., Grest, G. S. and Kremer, K. “Statics and Dynamics of Symmetric Diblock Copolymers: A Molecular Dynamics Study” *Macromolecules* **32**, 595 (1999)

62. Allen, M. P. and Tildesley, D. J. *Computer Simulation of Liquids* Oxford University Press, 1987, New York

63. Bockstaller R., Lapetnikov Y., Margel S. and Thomas E. L. “Size-Selective Organization of Enthalpic Compatibilized Nanocrystals in Ternary Block Copolymer/Particle Mixtures” *J. Am.Chem. Soc.* **125**, 5276 (2003)
64. Lauter-Pasyuk V., Lauter H. J., Ausserre D., Gallot Y., Cabuil V., Kornilov E. I. and Hamdoun B. “Effect of nanoparticle size on the internal structure of copolymer-nanoparticles composite thin films studied by neutron reflection” *Physica B* **241**, 1092 (1998)
65. Chen, S., Huang, Y. Tsiang, R. C. “Ozonolysis Efficiency of PS-b-PI Block Copolymers forForming Nanoporous Polystyrene*” J. Polym. Sci. Part A: Polymer Chemistry* **46**, 1964 (2008)